Arctic Oscillation during the Mid-Holocene and Last Glacial Maximum from PMIP2 Coupled Model Simulations

JUN-MEI LÜ

Korea Polar Research Institute, KORDI, Incheon, South Korea, and Chinese Academy of Meteorological Sciences, Beijing, China

SEONG-JOONG KIM

Korea Polar Research Institute, KORDI, Incheon, South Korea

AYAKO ABE-OUCHI

Center for Climate System Research, University of Tokyo, Kashiwa, Japan

YONGQIANG YU

LASG, Institute of Atmospheric Physics, Chinese Academy of Sciences, Beijing, China

RUMI OHGAITO

Japan Agency for Marine-Earth Science and Technology, Yokohama, Japan

(Manuscript received 6 July 2009, in final form 26 February 2010)

ABSTRACT

Changes in the Arctic Oscillation (AO) during the mid-Holocene and the Last Glacial Maximum were compared to preindustrial (PI) simulations using four coupled ocean–atmosphere models [i.e., Community Climate System Model (CCSM), third climate configuration of the Met Office Unified Model (HadCM3) Met Office Surface Exchanges Scheme, version 2 (MOSES2), L'Institut Pierre-Simon Laplace (IPSL), and Model for Interdisciplinary Research on Climate 3.2 (MIROC3.2)] from the second phase of the Paleoclimate Modeling Intercomparison Project. Results show that the amplitude of the simulated AO during the mid-Holocene is a little smaller than that of the preindustrial simulation. Although the AO pattern and vertical structures are similar to those in the preindustrial simulation, the polar westerlies are slightly weakened and displaced downward to the lower stratosphere, accompanied by weakening of the polar vortex and warming of the cold polar cap region. During the Last Glacial Maximum, when the Northern Hemisphere experiences severe cooling, the intensity of the AO decreases substantially compared to the mid-Holocene, with smaller standard deviations of the AO indices in all models. Furthermore, the magnitude of positive and negative centers of the AO spatial pattern decreases and the strength of the polar vortex and westerlies weakens further with the center of westerlies displaced into the midlatitude upper troposphere. The polar cap region becomes anomalously warm in the stratosphere, whereas it remains cold in the troposphere. The AO appears to be sensitive to background climate state.

Upward-propagating stationary Rossby waves are found to be stronger during the mid-Holocene and Last Glacial Maximum than in the preindustrial simulation. This increase in planetary wave activity might be responsible for the simulated weakening of the AO during the mid-Holocene and Last Glacial Maximum. Recent studies have shown that there is a significant correlation between Eurasian fall snow cover and the winter AO. The upward propagation of Rossby waves was further proposed to explain the physical process linking the AO with the snow depth. It is suggested that a large increase in fall snow depth during the Last Glacial Maximum strengthens the upward-propagating stationary Rossby waves relative to the PI.

Corresponding author address: Seong-Joong Kim, Korea Polar Research Institute, 7-50 Songdo-Dong, Yeonsu-Gu, Incheon, 406-840, South Korea.
E-mail: seongjkim@kopri.re.kr

DOI: 10.1175/2010JCLI3331.1

1. Introduction

Current and future changes in the global climate have attracted concern worldwide. Projections of possible future climate changes can only be performed using numerical models of the earth system. The motivation for the Paleoclimate Modeling Intercomparison Project (PMIP) is to test the performance and reliability of state-of-the-art climate models in the past, when the external forcings were large and relatively well known and for which various types of geological evidence indicate what actually happened in terms of climate. In the initial phase of the project (PMIP1), atmospheric general circulation models (AGCMs) were used to simulate the climate during the Last Glacial Maximum [LGM; 21 000 yr before present (21ka BP)] and the mid-Holocene [MH; 6000 yr before present (6ka BP)]. Many features of the paleoclimate are reproduced by all models and paleoenvironmental observations (PMIP 2000), even though the magnitude of the response varies among different models. The second phase of the project (PMIP2) was launched in 2002 (Harrison et al. 2002; Crucifix et al. 2005). Compared to PMIP1, PMIP2 considers a suite of numerical experiments that differ by the number of components of the earth system. Model–model and model–data comparisons of the PMIP2 coupled simulations have been performed to determine the ability of the models to reproduce past climates that differ from the climate of the present day, thereby increasing our understanding of climate change (Gladstone et al. 2005; Braconnot et al. 2007a; Brewer et al. 2007). Nevertheless, there are still significant discrepancies between different model results (Braconnot et al. 2007b; Weber et al. 2007; Zheng et al. 2008).

The Arctic Oscillation (AO) is a dominant mode of atmospheric variability in the Northern Hemisphere (NH). A large number of studies have revealed that the AO is an important determinant of the winter climate at middle and high latitudes in the NH (Kerr 1999; Thompson and Wallace 2000, hereafter TW00; Thompson and Wallace 2001; Gong et al. 2001; Wu and Wang 2002). Because of its dramatic impacts on the NH climate, which directly affect human societies, the AO has received much attention over the past decade. The vertical structure of the AO and the surface temperature pattern associated with the AO were demonstrated based on observed data (Thompson and Wallace 1998, hereafter TW98; TW00). Furthermore, possible physical mechanisms involved in maintaining the AO, such as stratosphere–troposphere interactions, eddy-mean flow feedback, and planetary wave activity, have been proposed (DeWeaver and Nigam 2000; Saito et al. 2001; Chen and Huang 2005; Lü et al. 2008). According to the theory of wave-mean flow interaction (Andrews et al. 1987), when planetary wave activity is weak in the middle latitude stratosphere, the decline of dynamic adiabatic heating in polar cap regions leads to a decrease in temperature, the increase of meridional temperature gradient, the acceleration of the polar night jet, and finally the strengthening of stratospheric AO. In recent years, it has been revealed that there is a significant negative correlation between Eurasian–Tibetan Plateau fall snow cover and the winter AO. Moreover, the upward propagation of Rossby waves was proposed to explain the physical process linking the AO with the snow depth (Saito et al. 2001; Cohen et al. 2007; Lü et al. 2008).

It has been suggested that the observed positive AO trend in the past 20 yr has contributed significantly to the observed warming over Eurasia and North America (Thompson et al. 2000; Thompson and Wallace 2001). Several authors have speculated that the reduction of planetary wave activity might be responsible for the stronger, colder stratospheric Arctic vortex based on observed data (Newman et al. 1997; Waugh et al. 1999). Using climate models that include a realistic representation of the stratosphere, Shindell et al. first reported in 1999 that an anthropogenically mediated increase in stratospheric greenhouse gas concentrations might

TABLE 1. PMIP2 OAGCM characteristics and references.

PMIP2 name	Abbreviation	Model designation	Length (unit: yr)			Reference for model
			0ka	6ka	21ka	
CCSM3	CCSM	Community Climate System Model run at NCAR (Boulder, Colorado)	100	100	100	Otto-Bliesner et al. (2006)
HadCM3M2	HadCM3M2	Met Office Hadley Center model (United Kingdom)	100	100	100	Gordon et al. (2000)
IPSL-CM4-V1-MR	IPSL	IPSL model run at Le Laboratoire des Sciences du Climat et l'Environnement (LSCE; France)	100	100	100	Marti et al. (2005)
MIROC3.2-mocat	MIROC	CCSR, National Institute for Environmental Studies (NIES), and Frontier Research Center for Global Change (FRCGC) (Japan)	100	100	100	Hasumi and Emori (2004)

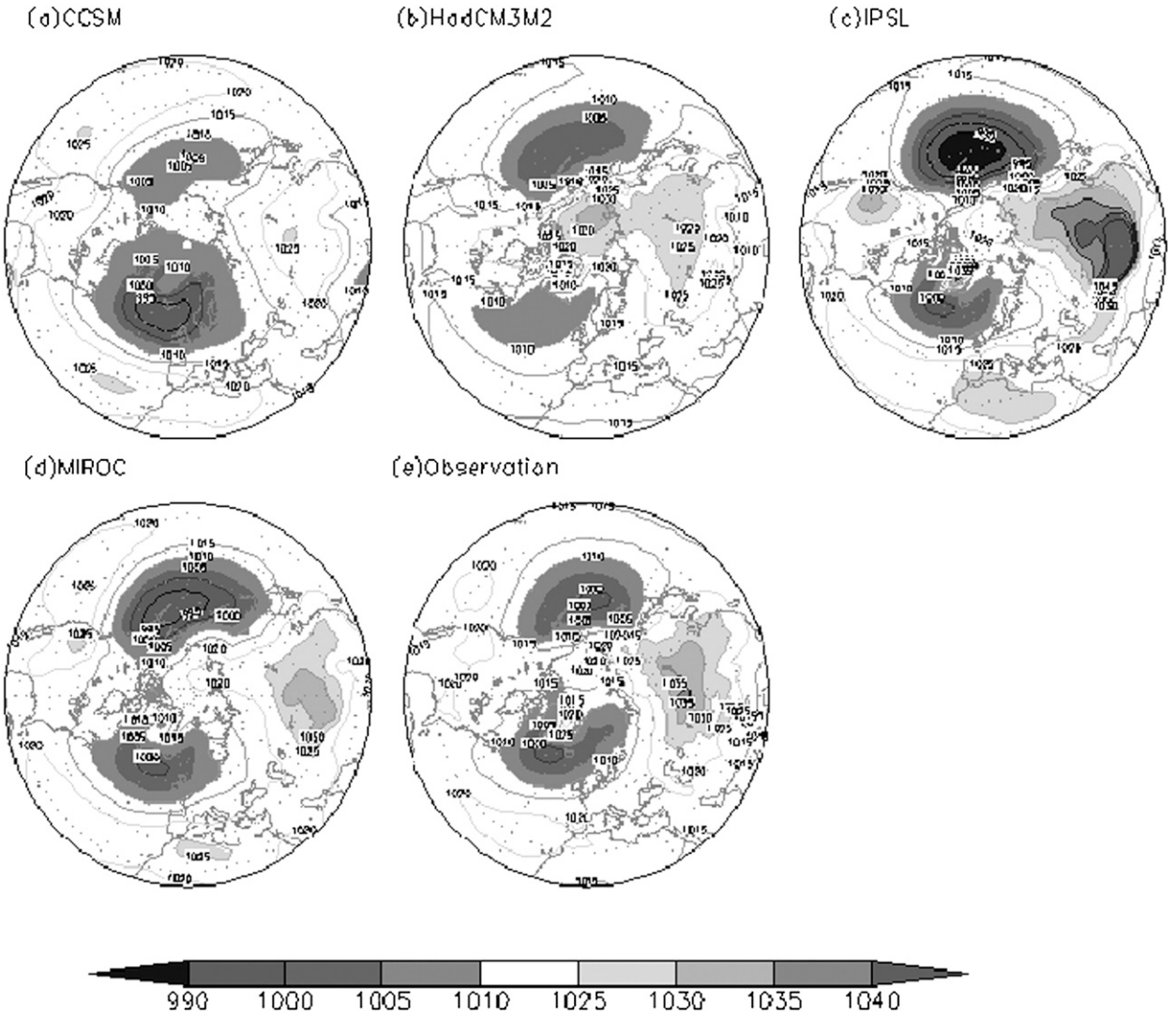

FIG. 1. Climatology of DJF SLP according to four models for the PI and observations. The contour interval is 5 hPa.

be responsible for the recent positive AO trend in the stratosphere and consequently the troposphere. Hu and Tung (2003) proposed that Arctic ozone depletion has caused the reduction in planetary wave activity in both the stratosphere and troposphere since the 1980s. Such a reduction in wave activity might be responsible for the observed winter and spring warming over NH high-latitude continents that is associated with the positive trend of the AO during the past two decades.

Furthermore, IPCC scenario A runs predicted continuation of the recent positive AO/North Atlantic Oscillation (NAO) trend until the middle of the twenty-first century (Paeth and Hense 1999). In contrast, Fyfe et al. (1999) argued that the modeled AO/Antarctic Oscillation (AAO) in a warmer world has not changed essentially but rather is superimposed on the forced climate change. Based on analysis of observed data, Cohen and Barlow (2005) argued that the global warming trend over the last 30 yr is unrelated to the AO and NAO. Thus, the relationship between AO and global warming is still unclear, and it is important to gain insight into the behaviors of the AO in different climate regimes. Analysis of past climates provides a unique opportunity that can help further understand the AO in response to CO_2 forcing in the future as different sources of the AO variations. To evaluate whether the climate models can correctly represent changes in the AO under different climate regimes, several studies have examined modeled AO/NAO variability during the MH and LGM. A PMIP2 model intercomparison showed a shift in the mean state of the climate toward a more positive NAO regime during the MH compared to preindustrial (PI; 0ka) control runs

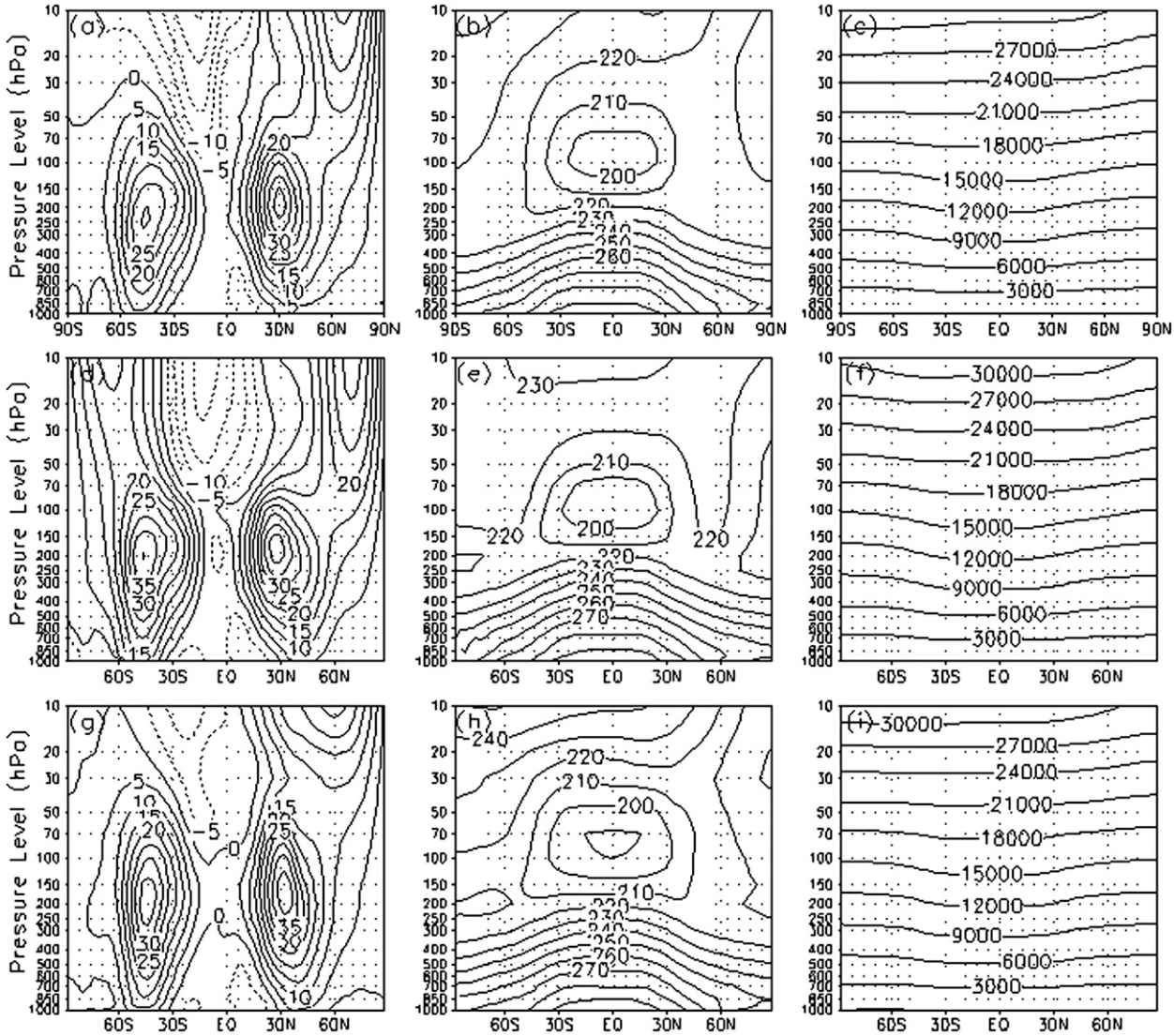

FIG. 2. Boreal winter climatology of (a),(d),(g) zonal-mean zonal wind (m s^{-1}); (b),(e),(h) temperature (K); and (c),(f),(i) geopotential height (m) for (top) observation, (middle) CCSM during the PI, and (bottom) MIROC during the PI.

(Gladstone et al. 2005). The AO during the MH and LGM in the Community Climate System Model, version 3 (CCSM3) simulation was discussed by Otto-Bliesner et al. (2006). They proposed that the MH AO pattern is similar to PI in CCSM3; for the LGM, however, the centers of AO variability are shifted and weakened.

The behavior of the AO in different climate states, including warmer (future) and colder (LGM) regimes, was primarily discussed in the aforementioned works. However, further studies are required to investigate the changes in the AO structure and amplitude during paleoclimatic periods according to various models. Furthermore, it has yet to be determined whether changes in MH and LGM AO result from stationary wave anomalies caused by some external forcing. The objectives of this paper are to investigate changes in the AO during the LGM and MH and to gain a better understanding of the physical mechanisms driving the AO.

2. PMIP2 experimental design and models

PMIP2 has thus far been implemented to investigate two representative climate intervals: namely, the LGM and MH. A strict protocol to run the LGM and MH experiments has been provided by the PMIP2 (available online at http://pmip2.lsce.ipsl.fr). The LGM simulation was designed to examine climate responses to the presence

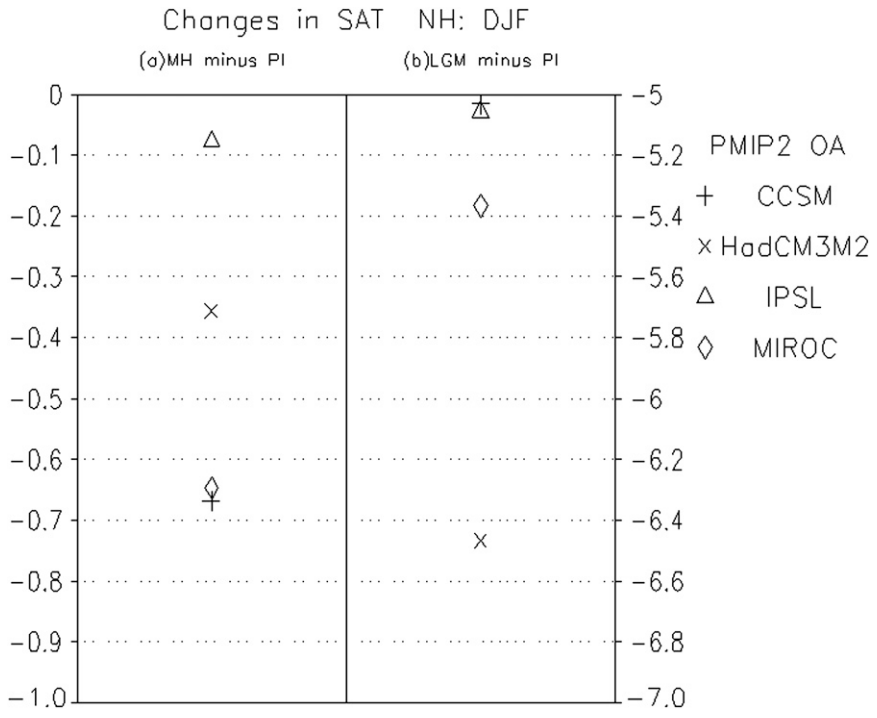

FIG. 3. Changes in the NH mean SAT (K) in DJF from PMIP2 OAGCMs experiments for (a) MH minus PI and (b) LGM minus PI.

of large ice sheets, lower sea levels, and lower greenhouse gas concentrations. The MH simulation was designed to investigate climate response to a primary forcing change in the seasonal and latitudinal distribution of incoming solar radiation (insolation) caused by known changes in orbital forcing (Berger 1978). The reference (control) simulation is a PI-type climate.

Results from coupled ocean–atmosphere models (OAGCMs) are considered in this paper. The available models for the LGM are not identical to those for the MH in PMIP2. Here, we will examine the LGM and MH AO using four models that provide data for both periods. Model information is provided in Table 1. The coupling procedure and the spinup strategy are model dependent and are described in the references of the models (Table 1). For each experiment, the models are run for a sufficient length of time to be representative of an equilibrium climate. Monthly values of the last 100 yr of integration are consistently used in analyses for all models. The vertical levels archived in the PMIP2 database are at 850-, 500-, and 200-hPa pressure surfaces for all models but the CCSM model, which has the fine vertical revolution of 17 levels from 1000 to 10 hPa. In this paper, the vertical structure of the AO is analyzed using the CCSM and Model for Interdisciplinary Research on Climate (MIROC) model simulations, because these are the only two models that provide atmospheric data with fine vertical resolution.

To assess model performance for the control simulation (PI simulation), we use the monthly-mean National Centers for Environmental Prediction–National Center for Atmospheric Research (NCEP–NCAR) reanalysis data (Kalnay et al. 1996) for the period 1951–99.

3. Simulated mean climate in boreal winter

Results of TW00 have demonstrated that the AO exhibits the larger variability in boreal winter [December–February (DJF)] than other seasons; thus, the mean climate during DJF will be the primary focus of this paper. As a basis for evaluating the performance of climate models in the AO simulation, the long-term mean climate for the PI simulation is discussed in this section based on the 100-yr integration.

a. Long-term mean climate during the PI era

Figure 1 shows the climatology of DJF sea level pressure (SLP) simulated by four models for the PI simulation together with the corresponding modern observations (1951–99). The observed DJF SLP shows two regions of lower SLP in the North Atlantic and North Pacific

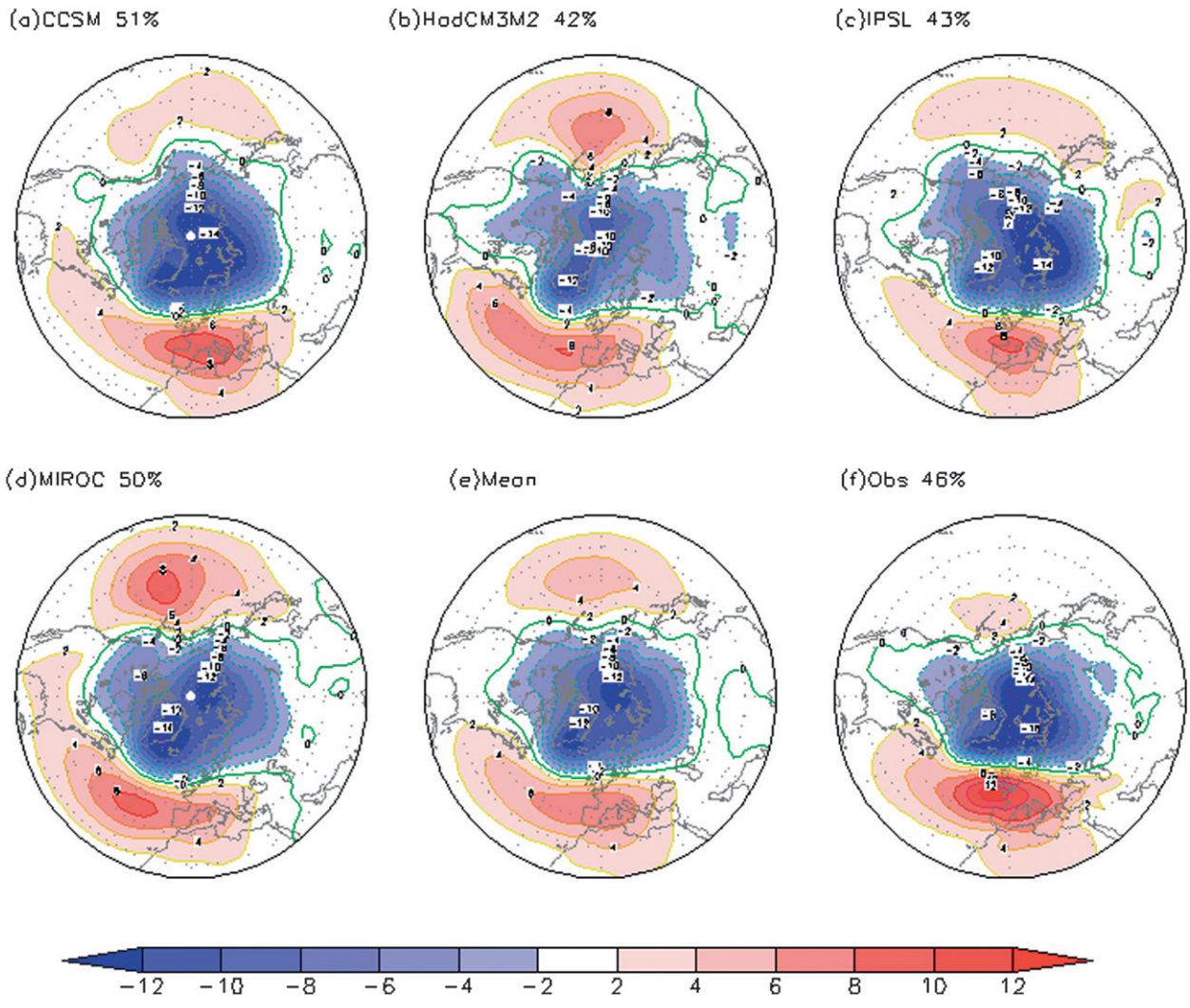

FIG. 4. Leading EOF shown as regression map of winter SLP simulated for the PI and observation. The contour interval is 2 hPa. The percentage of explained variance is shown at the top of each map.

corresponding to Icelandic and Aleutian lows, respectively, and a higher SLP region over the Eurasian continent associated with the Siberian–Mongolian high. The simulated high and low are stronger in L'Institut Pierre-Simon Laplace (IPSL) but weaker in CCSM than the observed high and low. The center of the Siberian–Mongolian high is shifted northward to polar areas in the third climate configuration of the Met Office Unified Model (HadCM3M2). Nevertheless, the winter SLP simulated using the four models is largely plausible. Climatological winter surface air temperature (SAT) in the PI simulation is very similar to the observed SAT (figure not shown). The simulated climatological winter SAT decreases with latitudes. The largest cooling centers are distributed over polar areas, including Greenland, northern North America, and Siberia. There is another cooling center over the Tibetan Plateau because of the snow cover. The primary comparison shows that four models are capable of simulating the present-day mean winter climate reasonably well. More detailed comparison of the simulated present-day mean climate with observations is beyond the scope of this paper.

Figure 2 displays the observed and simulated climatology of the zonal-mean zonal wind, temperature, and geopotential height in boreal winter. The observed results are shown in the top panels. The corresponding mean climates simulated by the CCSM and MIROC for the control simulation are displayed in the middle and bottom panels, respectively. It is obvious that the two models capture the large-scale distribution of the zonal-mean circulation, such as bihemispheric westerlies in the midlatitude upper troposphere, a polar night jet,

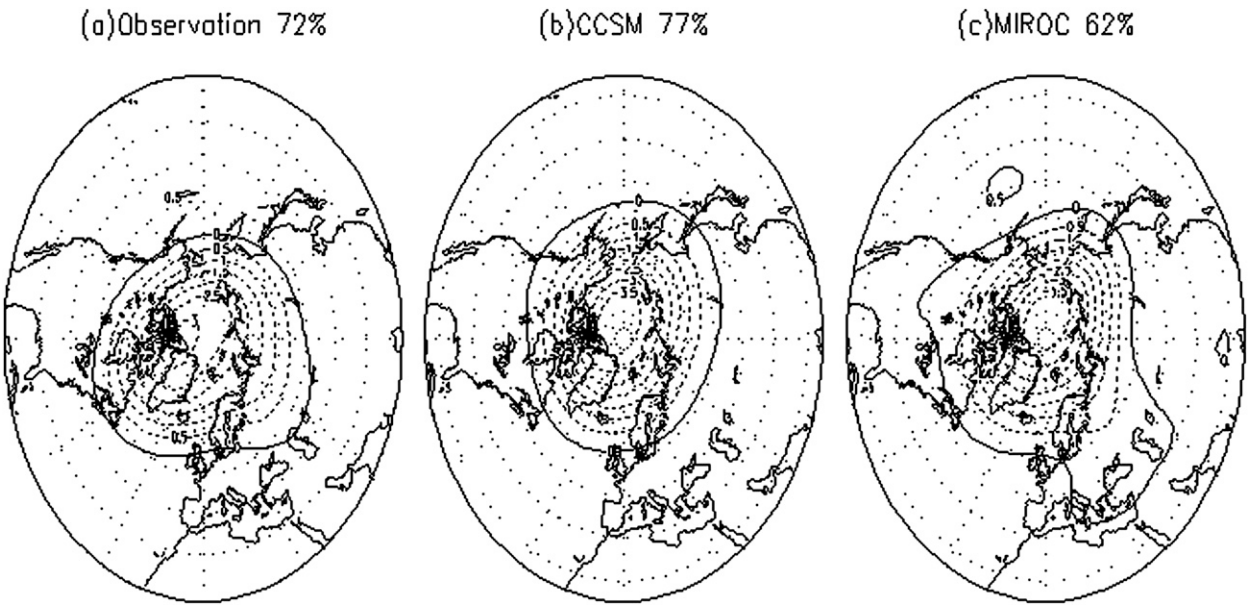

FIG. 5. Leading EOF of winter 50-hPa geopotential height anomalies for (a) observation, (b) CCSM during the PI, and (c) MIROC during the PI.

easterlies in the Southern Hemisphere middle stratosphere of low latitude, and a cold temperature center at the equatorial tropopause. Furthermore, the values obtained from simulations using the two models are in agreement with observations. These results suggest that both CCSM and MIROC can resolve stratospheric dynamics accurately. Shindell et al. (1999) proposed that inclusion of a well-resolved stratosphere in climate models is essential to accurately reproduce the observed trend in the AO.

b. Changes in NH mean DJF SAT for the MH and LGM

Based on proxy data and the PMIP2 simulations, several studies compared the MH and LGM climate changes over the ocean and continent. It was revealed that, although the same characteristics of temperature changes suggested by the reconstructions are reproduced in most models, the spatial distribution of temperature anomalies are not at the right location exactly (Kageyama et al. 2006; Brewer et al. 2007). Otto-Bliesner et al. (2006) demonstrated that the LGM CCSM3 simulation has a global cooling of 4.5°C compared to the PI, whereas the MH CCSM3 simulation has a global, annual cooling of less than 0.1°C compared to the PI simulation.

We examined the changes in NH mean DJF SAT for the MH and LGM in comparison with the PI era. The major difference between the MH and PI arises from the orbital configuration. The MH simulation has a small NH winter cooling less than 1.0 K for all models because of lower insolation than during the PI (Fig. 3a). Proxy records also revealed that winter temperatures in Europe were lower throughout the Holocene (Davis et al. 2003) compared to the present day. In the LGM, a marked surface cooling is found in the NH associated with the expansion of large ice sheets and reduced greenhouse gas concentrations. All models simulated a large temperature decrease of more than 5.0 K in the NH (Fig. 3b). Proxy data derived from different paleoclimatic archives indicate the same degree of NH

TABLE 2. AO statistics for the PI, MH, and LGM.

	Percentages explained variance			AO amplitude			Mean values of positive/negative AO index		
Model	0ka	6ka	21ka	0ka	6ka	21ka	0ka	6ka	21ka
CCSM	51	56	48	166	181	111	126/–145	145/–148	88/–97
HadCM3M2	42	38	25	105	100	60	81/–90	79/–84	42/–53
IPSL	43	39	46	131	119	110	100/–115	92/–95	92/–93
MIROC	50	43	43	140	119	112	130/–100	93/–99	103/–82

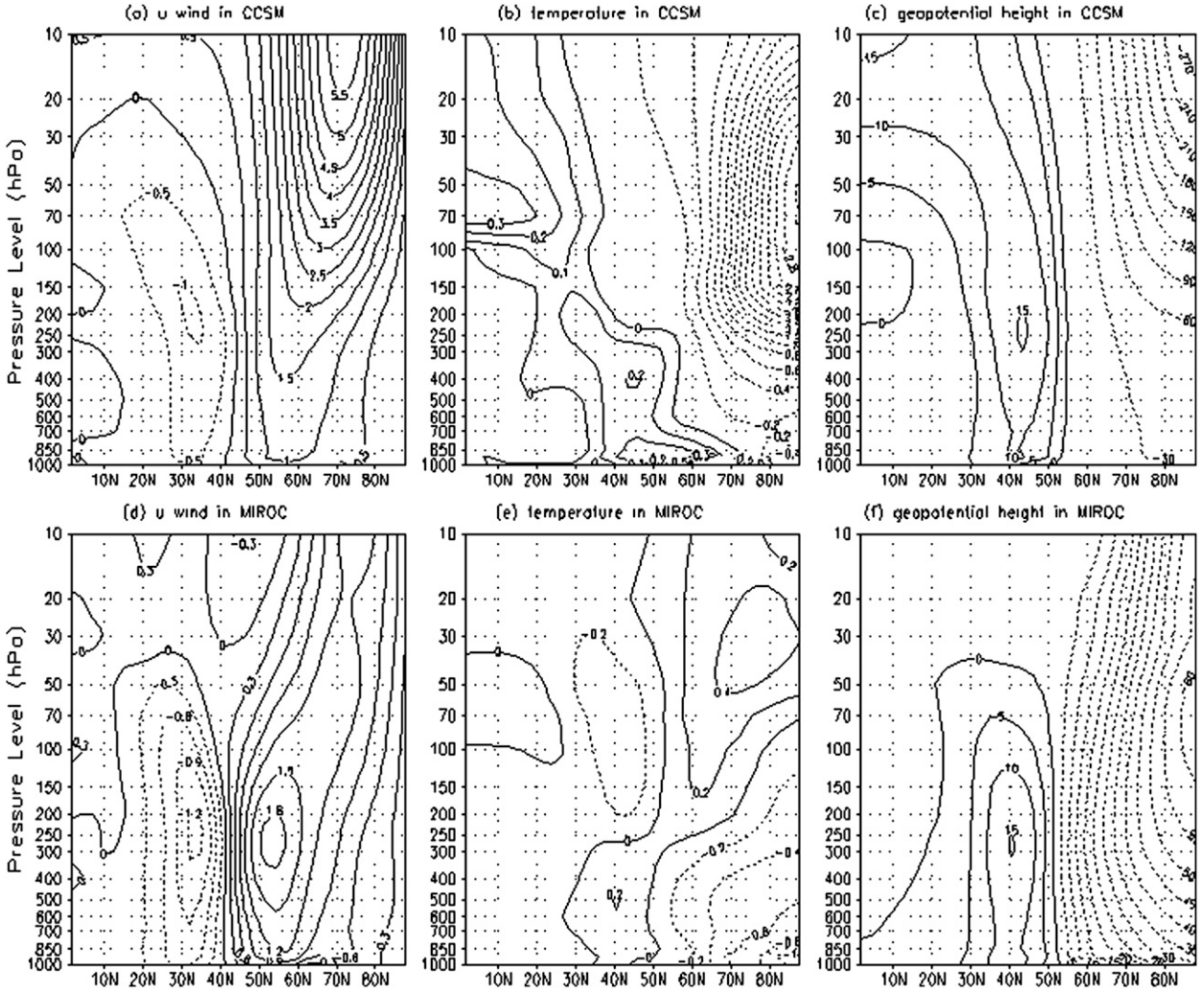

FIG. 6. (a),(d) Zonal-mean zonal wind; (b),(e) temperature; and (c),(f) geopotential height regressed on the standardized AO index for (top) CCSM and (bottom) MIROC during the PI. Units are in m s^{-1}, kelvins, and meters per STD of the respective index time series.

cooling in LGM winter (Kim et al. 2008). Overall, the winter mean climate is somewhat colder during the MH and much colder during the LGM than during the PI.

4. Simulated AO

Empirical orthogonal functions (EOFs) are commonly used to determine the dominant patterns of variability in a meteorological element. EOFs represent a number of fixed spatial patterns of a dataset, with each EOF multiplied by its time-varying amplitude [principal component (PC)]. These patterns are uncorrelated or statistically orthogonal to each other. The leading EOF of the extratropical SLP (20°–90°N) is referred to as the AO or Northern Hemisphere annular mode (TW98; TW00), which is a dominant mode of atmospheric variability in the NH. The AO index is defined as the time-dependent variation of the AO given by the first principal component (PC1).

a. Simulated AO in the PI simulation

In the PI simulation (control simulation), the leading EOF of DJF SLP explains 42%–51% of total variance for the four models with negative anomalies near the pole and positive anomalies at middle latitudes (Fig. 4), which are not model dependent. These are characteristics of a positive AO pattern termed by TW98. The modeled leading EOF closely resembles the observation (Fig. 4f), though the values of the positive and negative

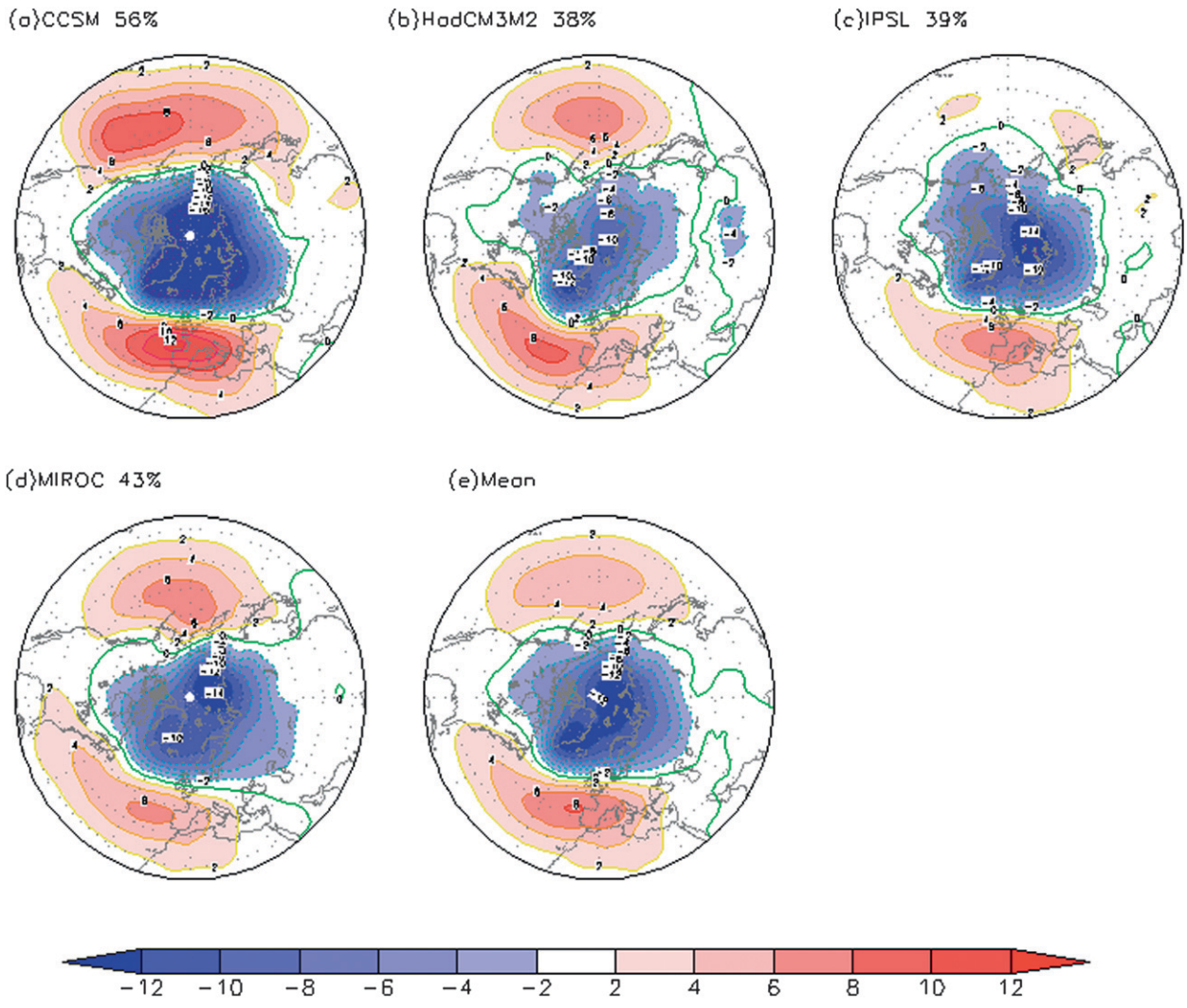

FIG. 7. As in Fig. 4, but for the MH.

centers vary across the different models. Figure 5 shows the leading EOF of winter 50-hPa geopotential height anomalies. The stratospheric AO signature manifests principally a feature of the polar vortex. It is noted that the simulated leading EOF patterns of 50-hPa height for CCSM and MIROC are virtually identical to that of the observation (Fig. 5a). These results suggest that both CCSM and MIROC are able to reproduce the AO from the stratosphere through the troposphere.

The standard deviation (STD) is a statistic used to measure the typical year-to-year fluctuation of a quantity. In this paper, the amplitude variability of the simulated AO is measured by the STD of the AO indices. The mean values of the positive and negative AO indices were calculated to measure the amplitude of the AO in each phase. These AO statistics are listed in Table 2. Even though all models produce similar AO patterns in SLP, the magnitudes of the AO amplitude are different. The AO amplitude varies from 105 in HadCM3M2 to 166 in CCSM (Table 2).

As documented by TW00, the vertical structures of the AO can be extracted by regression analysis. In this paper, the analyses of simulated vertical AO structure are based on two PMIP2 models: namely, the CCSM and MIROC. The zonal-mean zonal wind, geopotential height, and temperature were regressed on the standardized AO index for the domains from equator to pole and from 1000 to 10 hPa (Fig. 6), respectively. Because the analysis is linear, regression maps are described in terms of the positive polarity of the AO.

For CCSM, the zonal-mean zonal wind associated with the AO is characterized by easterly anomalies at middle latitudes and westerly anomalies at high latitudes (Fig. 6a). The maximum easterly anomalies are found at

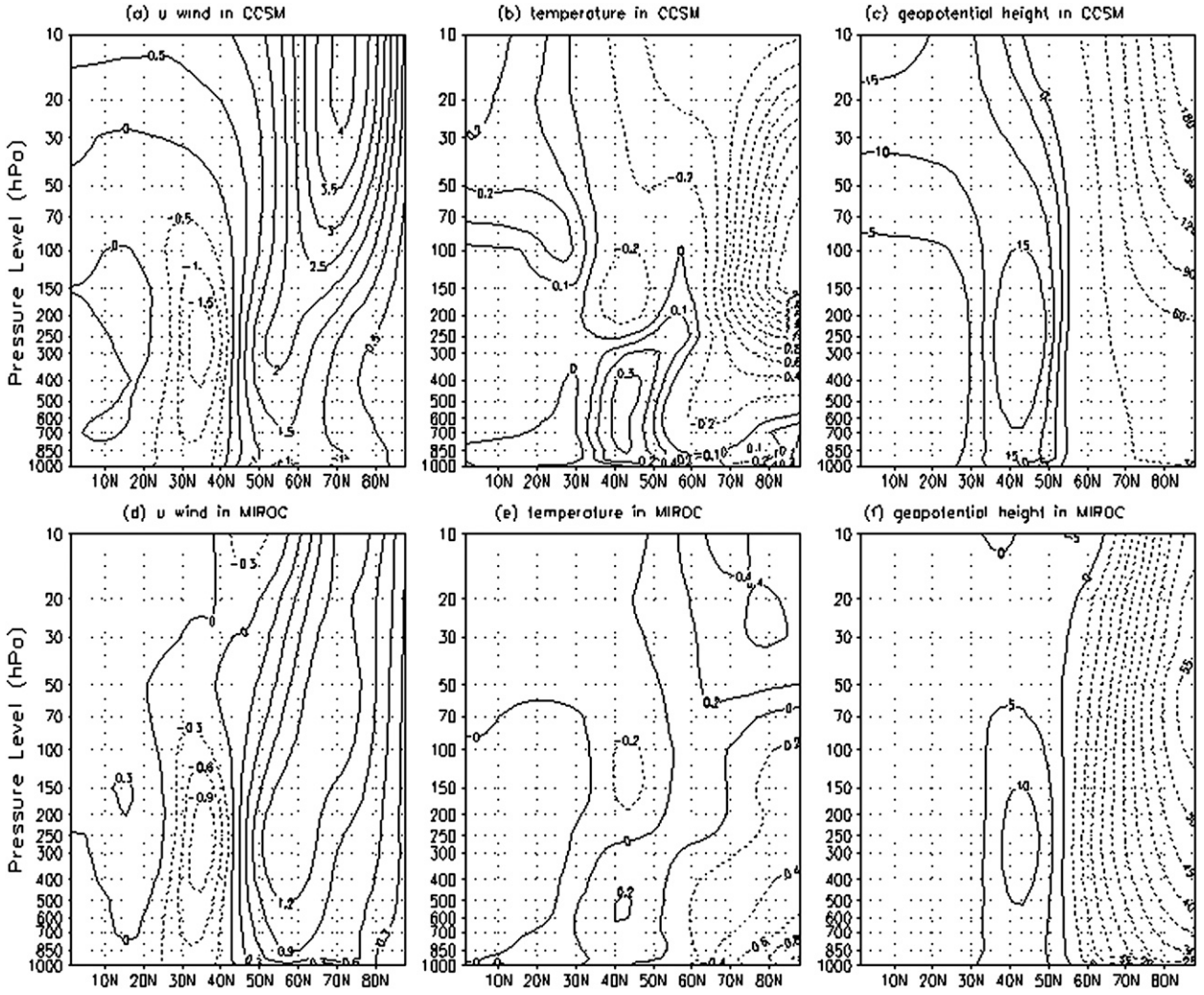

FIG. 8. As in Fig. 6, but during the MH.

~33°N at the 200-hPa level, whereas the westerly anomalies amplify with height from the surface upward into the middle stratosphere. Simultaneously, the axis tilts slightly poleward from ~58°N in the lower troposphere to ~73°N at the 10-hPa level. The maximum westerly anomalies appear in the polar upper stratosphere. Figure 6b shows the zonal-mean temperature regressed onto the AO index. The positive polarity of the AO is marked by an anomalously cold polar cap region throughout the atmospheric column, indicative of adiabatic cooling. The negative temperature anomalies display a center extending from the tropopause to the lower stratosphere. The positive temperature anomalies extend upward and equatorward from the midlatitude troposphere to the tropical lower stratosphere. Correspondingly, the zonal-mean geopotential height in association with the positive AO manifests as negative height anomalies at high latitudes throughout the atmospheric column and positive height anomalies extending from the midlatitude troposphere to the tropical middle stratosphere (Fig. 6c), indicative of the barotropic structure of the AO.

In the PI simulation, the vertical structures of the AO modeled by CCSM are virtually identical to that derived from present-day observations (see Fig. 7 of TW00). This indicates that the CCSM model accurately captures the AO signature in the lower and middle stratosphere.

The vertical structures of the AO simulated using MIROC (Figs. 6d–f) exhibit some differences from the observed results of TW00. The zonal-mean geopotential height (Fig. 6f) and zonal wind (Fig. 6d) associated with the AO still appear as negative height anomalies and westerly anomalies at high latitudes from surface to stratosphere, respectively, although the maximum centers

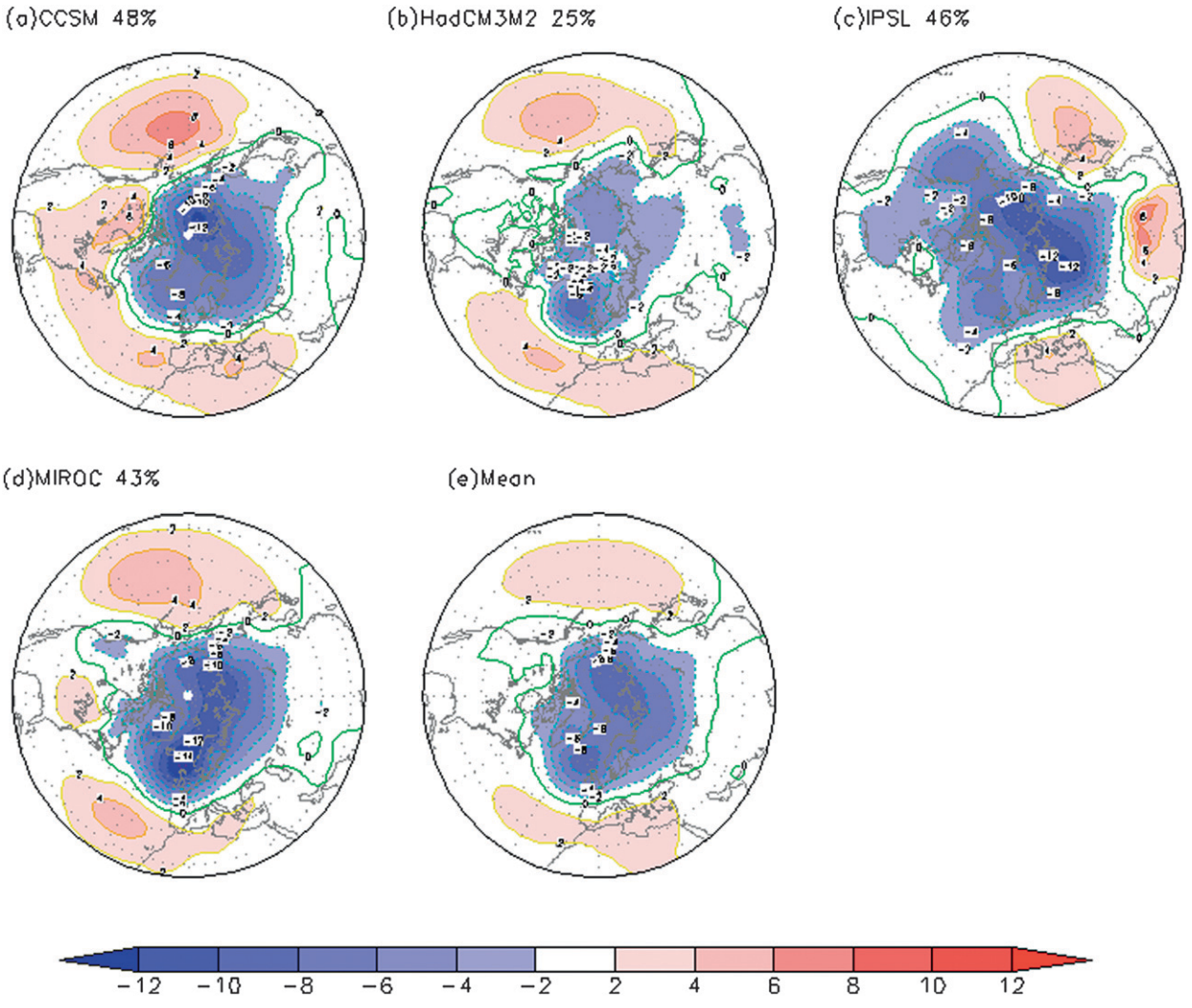

FIG. 9. As in Fig. 4, but for the LGM.

are shifted downward to the upper troposphere from the upper stratosphere. The AO-related temperature (Fig. 6e) shows baroclinic characteristics with the positive anomalies in the high-latitude stratosphere but negative anomalies in the high-altitude troposphere. This corresponds to the previously mentioned downward shift of the maximum westerly centers. The MIROC is able to reproduce the main characteristics of the vertical structure of the AO, even though there are some discrepancies from the observations (see Fig. 7 of TW00).

b. Changes in the AO during the MH

During the MH, the leading EOF of DJF SLP is similar to the PI; that is, there is a pronounced dipole over the North Atlantic corresponding to the NAO and a weaker dipole over the North Pacific (Fig. 7). Otto-Bliesner et al. (2006) obtained the same result in their CCSM3 experiments. Because it is almost impossible to distinguish the changes in MH AO from that of the PI according to EOF1, more in-depth comparisons are needed. The percentage of explained variance and the AO amplitude at the MH are slightly reduced compared to the PI in all models except for CCSM (Table 2). Accordingly, the absolute magnitudes of the mean values of the positive and negative AO indices are smaller than that of the PI (Table 2) in all models except for CCSM (Table 2). These results indicate that the variability of the AO is damped slightly during the MH relative to the PI period. A continuous weakening of the AO/NAO pattern from the early to late Holocene was also detected in proxy data based

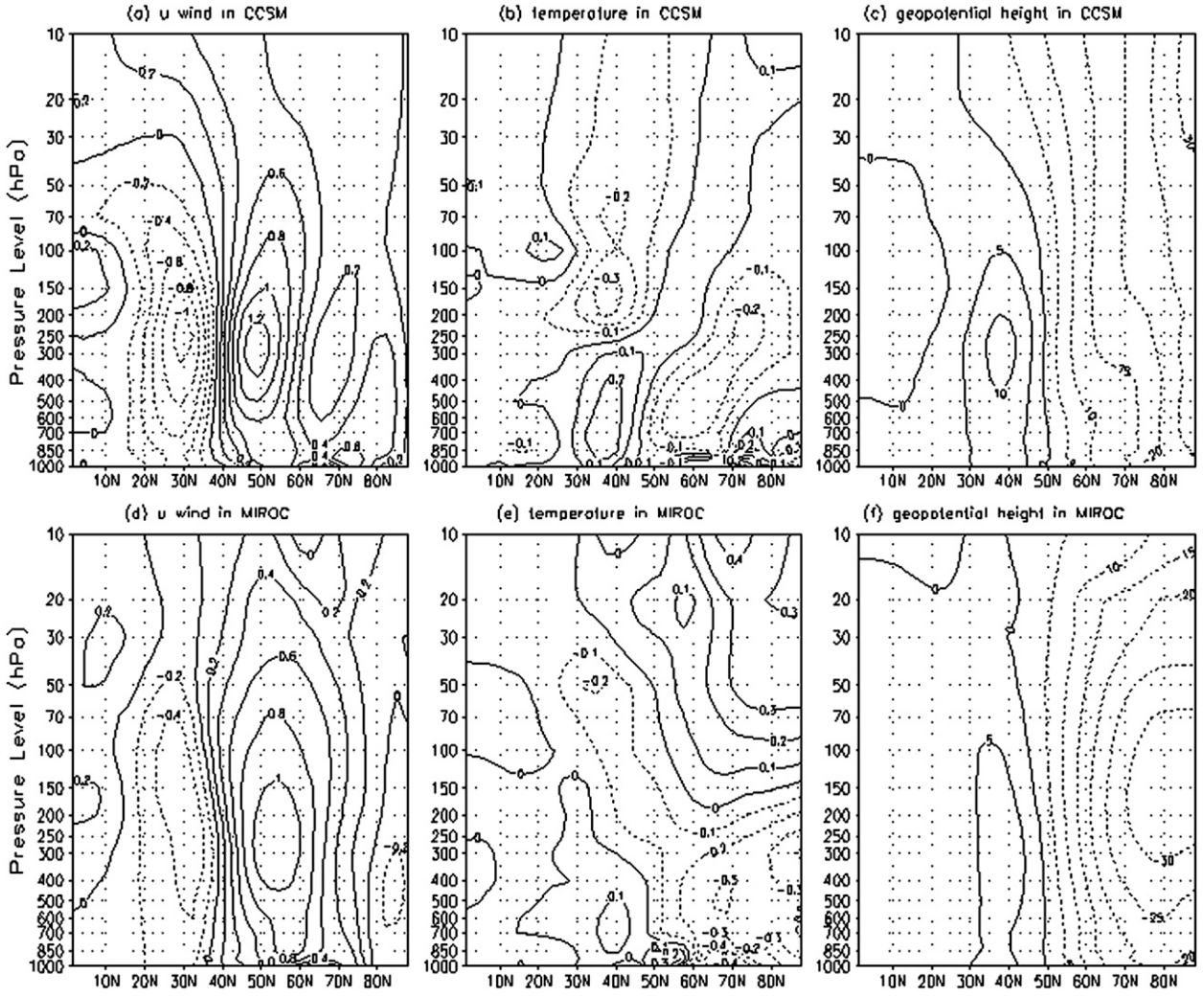

FIG. 10. As in Fig. 6, but during the LGM.

on alkenone-derived SST reconstructions (Rimbu et al. 2003).

A decrease in AO intensity during the MH is also found in the zonal-mean vertical structure (Fig. 8). The vertical structures of the AO during the MH resemble those during the PI, but discrepancies are also evident. In CCSM, the westerly anomalies are reduced with the center displaced downward and equatorward from ~73°N at the 10-hPa level to ~70°N at the 20-hPa level (Fig. 8a). Meanwhile, the negative geopotential height (Fig. 8c) and temperature anomalies (Fig. 8b) of polar cap regions increase markedly relative to the PI, with the center of negative temperature anomalies shifted downward into the upper troposphere, indicating weakening of the polar vortex. In MIROC, the vertical structures of the AO at the MH (Figs. 8d–f) are similar to those at the PI. Nevertheless, the absolute values of the negative and positive centers are lower during the MH than the PI. Overall, these results suggest that AO intensity decreases slightly during the MH compared to the PI era.

c. *Changes in the AO during the LGM*

As shown in the previous section, there are few changes in the MH AO from the PI based on the leading EOF of SLP. However, during the LGM, the pattern of the leading EOF shows a substantial difference from that during the PI (Fig. 9). The negative centers in the Arctic are shifted to northern Eurasia and weakened compared to the PI, consistent with the results of Otto-Bliesner et al. (2006). Additionally, the positive zonal ring near 45°N is shifted southward (Fig. 9). The AO explains 25%–48% of SLP variation in the four models (Table 2). The calculated AO amplitude and the mean values of positive and negative AO indices (Table 2) also indicate that the

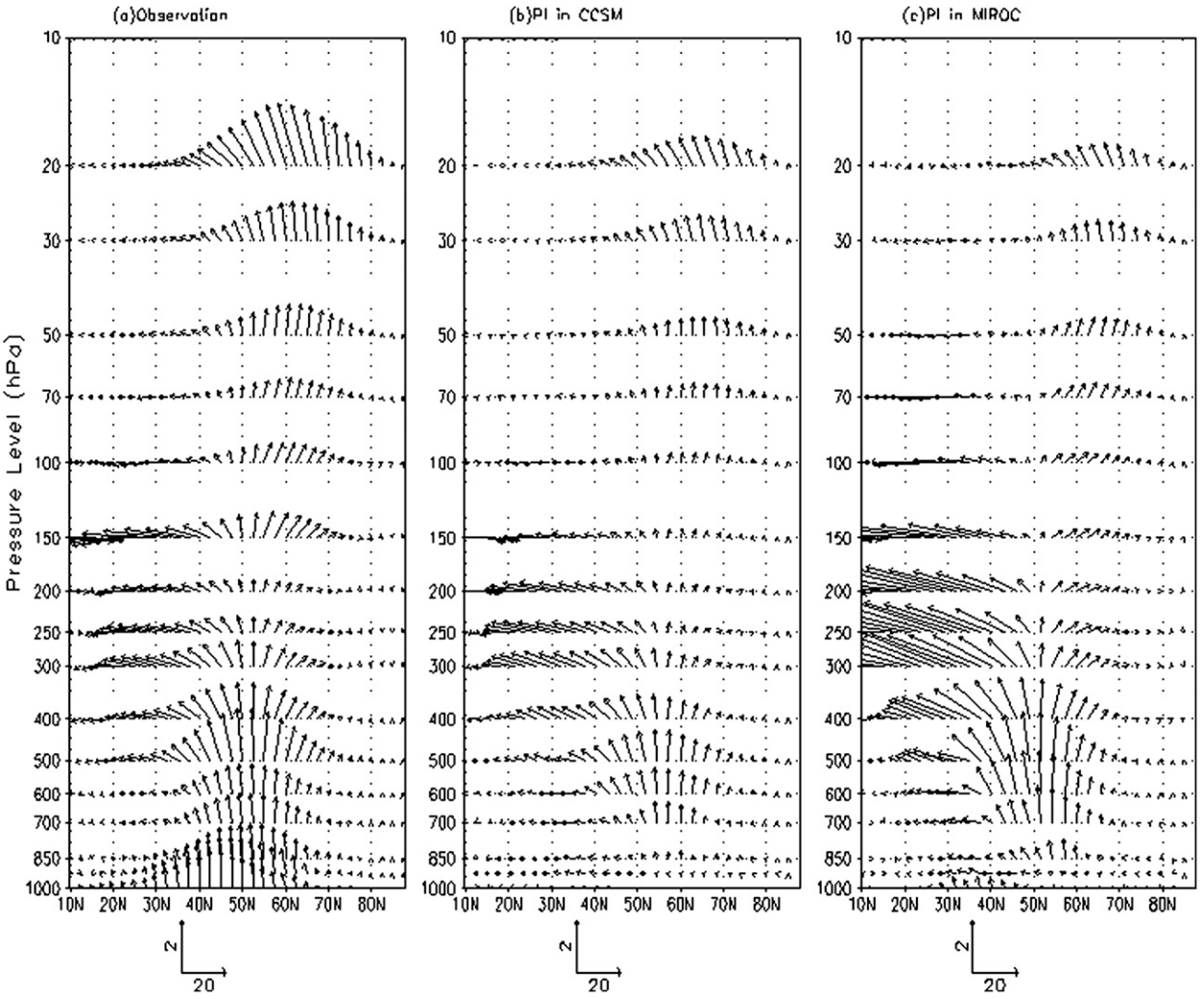

FIG. 11. E–P flux cross sections of average Rossby waves for (a) observation over 49 winters from the NCEP–NCAR reanalysis and the PI simulation over 100 winters from (b) CCSM and (c) MIROC. The horizontal (vertical) scale of arrows is shown at the bottom and represents 20 (2.0) $m^2 s^{-2}$.

AO during the LGM is weaker than that during the MH and PI.

The vertical structure of the AO simulated by CCSM during the LGM (Figs. 10a–c) exhibits significant differences from that during the PI. The center of negative geopotential height anomalies (Fig. 10c) displaces downward into the lower stratosphere and has a considerable weakening of more than 245 m in polar areas compared to the PI simulation. This indicates a decrease in intensity of the AO during the LGM. Both the westerly and easterly anomalies are shifted southward. Furthermore, the center of westerly anomalies is shifted downward from the high-latitude middle stratosphere to the midlatitude upper troposphere (Fig. 10a). The most striking differences in temperature (Fig. 10b) are indicated by two anomalous dipoles at middle and high latitudes. The former has a negative center in the upper troposphere and a positive center in the middle to lower troposphere, whereas the latter has a weak positive center at ~80°N at the 10-hPa level and a negative center extending from the midlatitude lower troposphere to the high-latitude upper troposphere. The anomalous dipoles of temperature are related to the weakening of the AO and the downward shift of the westerly anomalies.

Figures 10d–f show the vertical structures of the LGM AO as simulated by MIROC. Although the vertical structure is similar to that of the PI, absolute values of the maximum anomalies are smaller than those during the MH and PI, supporting weakening of the AO during the LGM as suggested by the CCSM model. It should

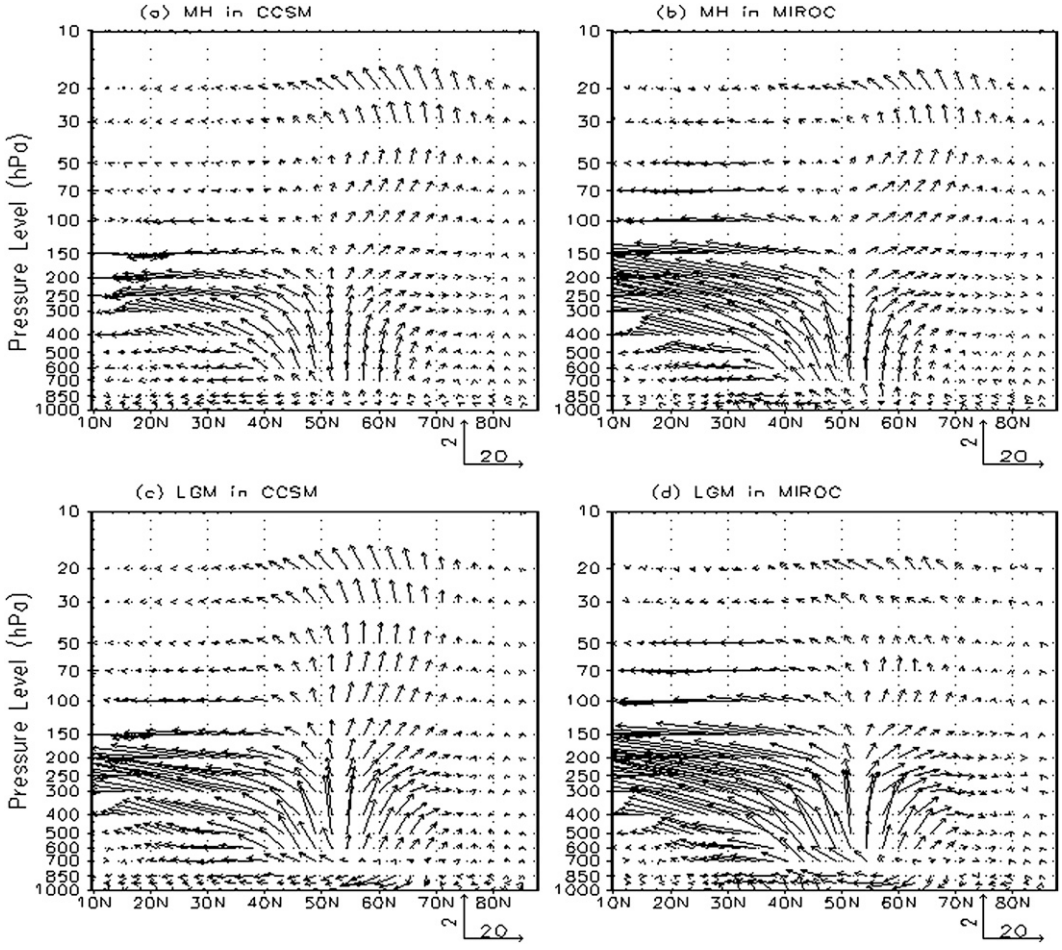

FIG. 12. E–P flux cross sections of average Rossby waves over 100 winters simulated for the MH in (a) CCSM and (b) MIROC and for the LGM in (c) CCSM and (d) MIROC. The horizontal (vertical) scale of arrows is shown at the bottom and represents 20 (2.0) $m^2 s^{-2}$.

also be noted that the LGM AO in CCSM appears to be almost completely confined to the troposphere (Fig. 10a), in contrast to current conditions (Fig. 6a) and those during the MH (Fig. 8a), which have the largest westerly signal in the upper stratosphere. This result clearly indicates a weaker stratospheric circulation during the LGM. Although this phenomenon is not obvious in MIROC, the center of negative geopotential height anomalies is shifted downward from the lower stratosphere at the PI (Fig. 6f) to the upper troposphere at the LGM (Fig. 10f), consistent with the results of CCSM.

d. What drives AO changes during the MH and LGM?

We found that the intensity of the simulated AO is slightly reduced during the MH when the NH winter is fairly cold, whereas it decreases markedly during the LGM when the climate is extremely cold. This suggests that the intensity of the AO is sensitive to the climate state. One dynamic mechanism that may be involved in maintaining the AO is the internal interaction between the zonal-mean flow and waves in the atmosphere. We therefore investigate the role of stationary Rossby waves on the weakening of the AO. The vertical propagation of the stationary Rossby waves are analyzed in terms of the wave activity flux (WAF), which is a three-dimensional extension of the Eliassen–Palm (E–P) flux defined by Plumb (1985). The wave activity fluxes were calculated using 17-level geopotential height, u wind, v wind, and temperature from NCEP–NCAR reanalysis, CCSM, and MIROC simulations.

Figure 11 shows the observed and simulated climatology of the vertical propagation of the stationary Rossby waves in boreal winter. Control simulations using the CCSM and MIROC models reproduce the primary features of the vertical propagation of stationary Rossby

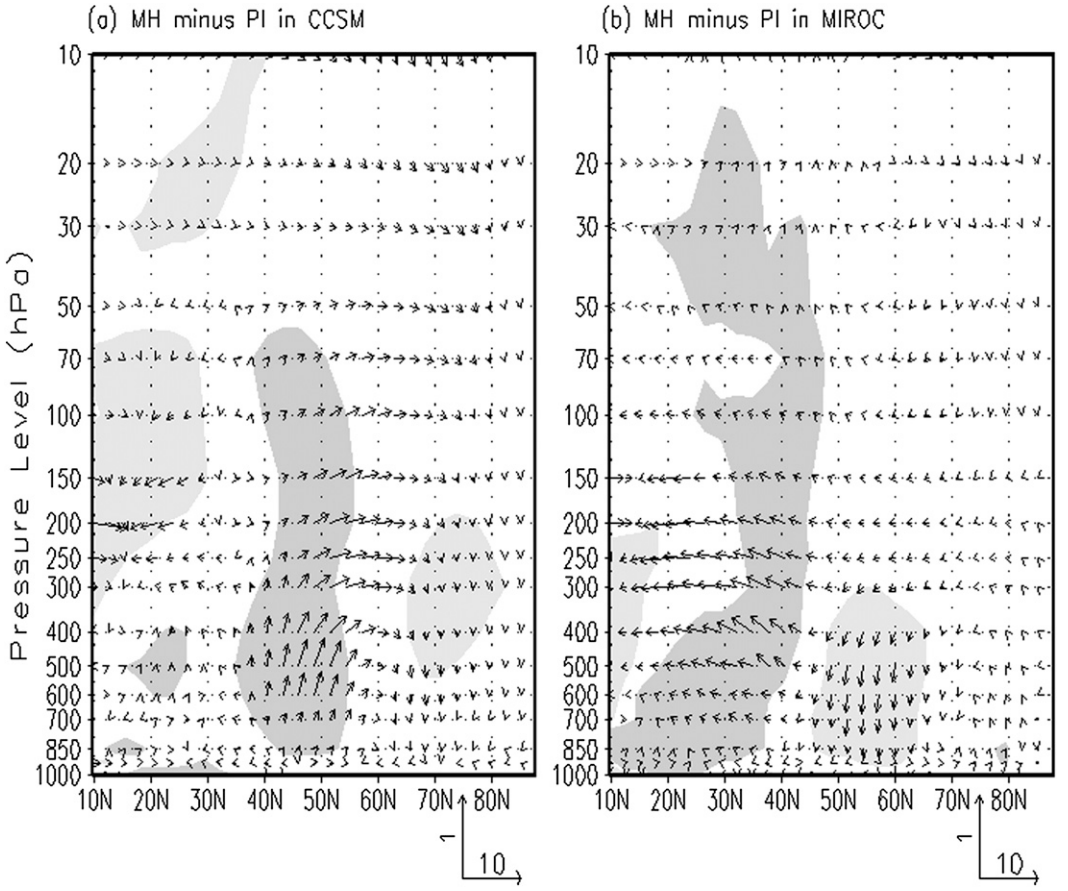

FIG. 13. Changes in the vertical propagation of Rossby waves during the MH compared to the PI in (a) CCSM and (b) MIROC simulations. Shaded areas indicate significant changes at 99% level, estimated by a local Student's *t* test. The horizontal (vertical) scale of arrows is shown at the bottom and represents 10 (1.0) $m^2 s^{-2}$.

waves (Figs. 11b,c). The stationary waves first propagate upward from the midlatitude lower troposphere and then propagate along two waveguides. One waveguide refracts toward high latitudes and propagates upward into the stratosphere, whereas the other refracts toward the equator in the troposphere. Except for the weaker polar waveguide, the features of E–P flux simulated by CCSM and MIROC in the control runs are consistent with the observations (Fig. 11a). This indicates that both CCSM and MIROC can simulate vertical E–P flux, even though the AO vertical structure simulated in MIROC has a small bias. The vertical propagation of the stationary Rossby waves during the MH (Figs. 12a,b) and LGM (Figs. 12c,d) exhibit similar features to those during the PI.

Figures 13a,b show changes in the vertical propagation of Rossby waves during the MH compared to the PI using both CCSM and MIROC models. The areas where the vertical component of E–P flux reaches the 99% confidence level are shaded. In the CCSM model, anomalous Rossby waves propagate upward and refract poleward in the middle troposphere through the lower stratosphere at middle latitudes (Fig. 13a), indicative of stronger upward propagation of Rossby waves during the MH compared with the PI. However, for MIROC, anomalous downward propagation in the high-latitude middle troposphere and equatorward propagation in the midlatitude upper troposphere are observed (Fig. 13b). It suggests that the upward-propagating stationary Rossby waves decrease during the MH relative to the PI.

CCSM (Fig. 14a) and MIROC (Fig. 14b) simulate identical changes in the vertical propagation of Rossby waves during the LGM. Although anomalous downward propagation occurs in the high-latitude stratosphere, significant anomalous upward propagation of Rossby waves prevails from the midlatitude middle troposphere through the stratosphere. It should also be noted that the

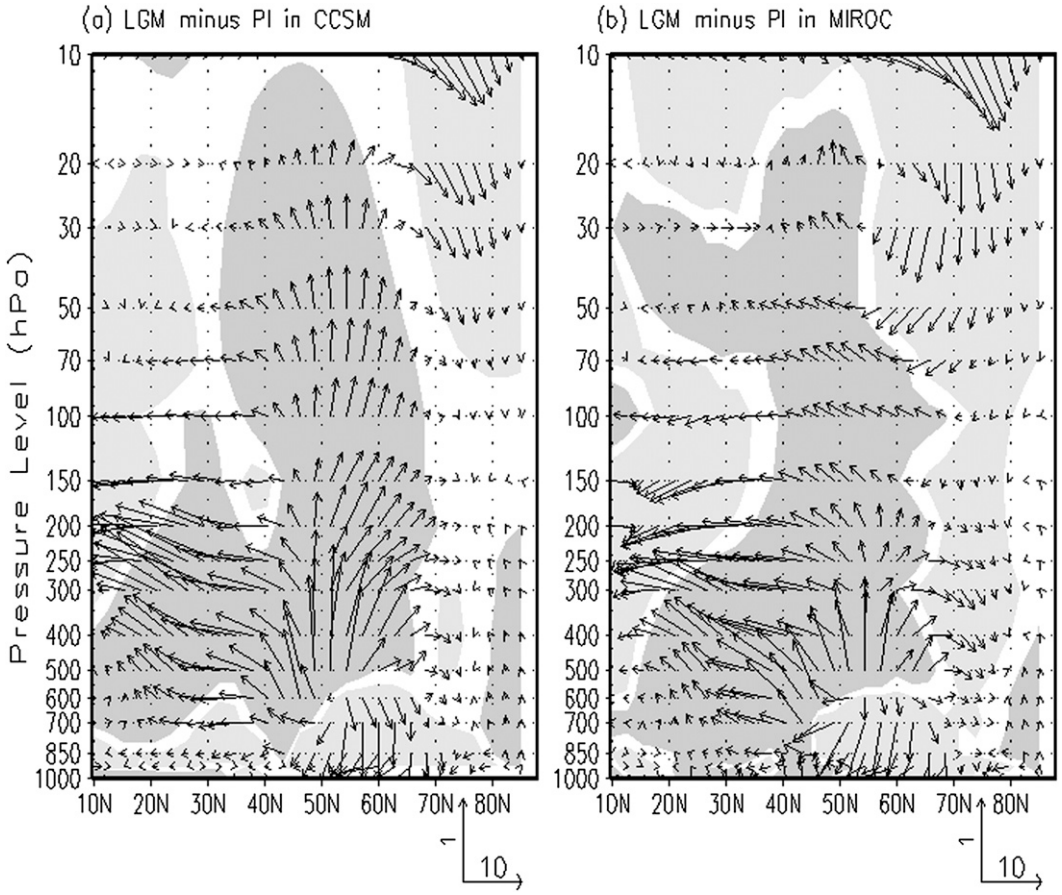

FIG. 14. As in Fig. 13, but during the LGM.

shaded areas expand largely during the LGM for two models (Fig. 14). This suggests that the anomalous upward propagation of Rossby waves is statistically significant from the midlatitude middle troposphere through the stratosphere; that is, the upward propagation of Rossby waves is much stronger during the LGM than the PI. According to the theory of wave-mean flow interaction, an enhancement of planetary wave activity weakens the stratospheric AO because of an increase in dynamic adiabatic heating of polar cap regions. In other words, during the LGM, stronger upward propagation of Rossby waves causes warming of polar stratosphere and then a decrease in meridional temperature gradient as shown in Figs. 10b,e. This finally results in a large weakening of the AO.

Generally, stationary Rossby waves always propagate upward because of topography and thermal contrast. In recent years, it has been demonstrated that Eurasian fall snow cover anomalies not only alter near-surface temperatures but also affect the upward propagation of Rossby waves (Cohen et al. 2007). The large fall snow extent over Eurasia induces diabatic cooling in the lower troposphere, amplifying orographically forced upward stationary waves. Ringler and Cook (1999) demonstrated that the presence of low-level cooling above the Tibetan Plateau tends to amplify both the mechanical forcing and the far-field stationary wave response. It is also proposed that latitudinal temperature gradient changes forced by snow cover lead to anomalous potential vorticity gradients in the stratosphere, which then alter the wave refraction index. As a result, an upward WAF anomaly responds almost immediately to the snow-forced thermal anomaly and appears in troposphere (Saito et al. 2001). Furthermore, some authors have proposed that Rossby wave changes forced in the stratosphere by anomalous fall snow cover are not identified until later in winter, when the troposphere and stratosphere are actively coupled (Cohen et al. 2007; Saito et al. 2001; Lü et al. 2008). Therefore, we investigate the effect of fall snow anomalies on the vertical propagation of Rossby waves during the MH and LGM winter.

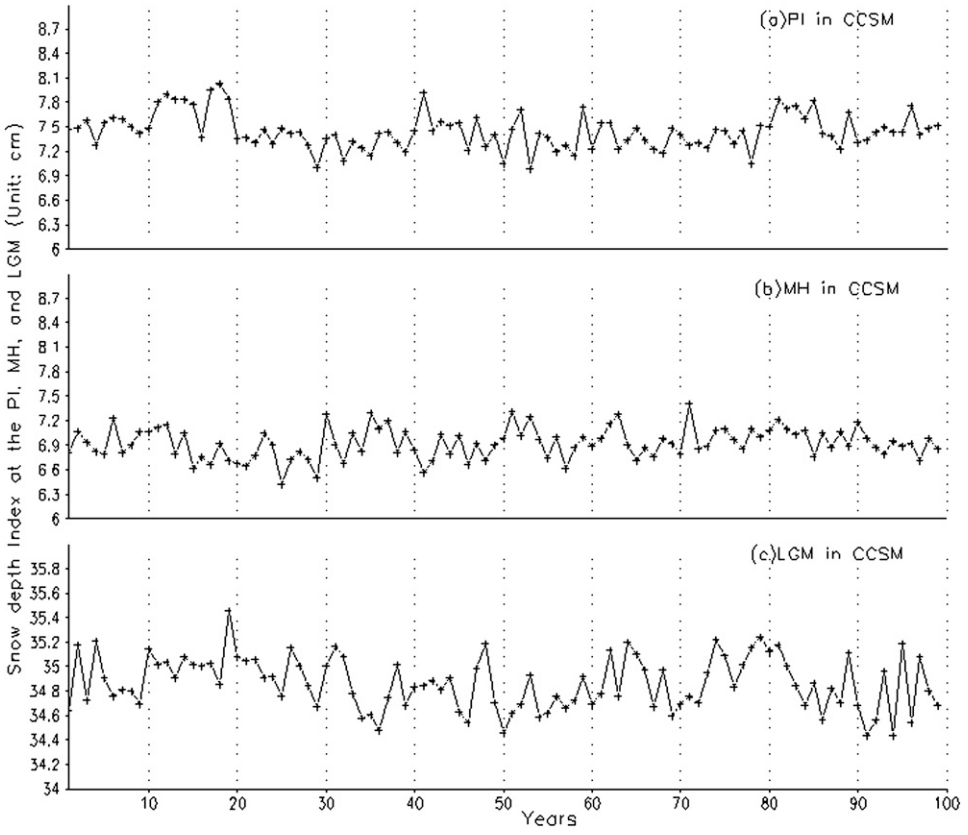

FIG. 15. Autumn snow depth indices for CCMS (cm) during the (a) PI, (b) MH, and (c) LGM.

We first define the fall snow depth index of NH by averaging the snow depth north of 50°N. Figures 15 and 16 indicate the fall snow depth indices during the PI, MH, and LGM for CCSM and MIROC, respectively. During the MH, the fall snow depth is similar to that during the PI for CCSM; however, in MIROC it is smaller than that during the PI. On the other hand, the fall snow depth is much greater during the LGM than that during the PI and MH for the two models.

To examine the role of snow depth on planetary wave activity, we calculated the regression coefficients of winter zonal-mean WAF on fall snow depth indices during the PI, MH, and LGM (Fig. 17). In CCSM, increased fall snow depth generates anomalous upward propagation of Rossby waves, which appears late in winter in the midlatitude troposphere through the stratosphere during the PI and MH (Figs. 17a,b), whereas during the LGM winter, anomalous upward-propagating Rossby waves prevail from the mid- and high-latitude troposphere through the stratosphere (Fig. 17c). In MIROC, the anomalous upward propagation of Rossby waves is also induced when the fall snow depth increases (Fig. 18). The anomalous Rossby waves propagate upward from the midlatitude troposphere through the stratosphere during the PI winter (Fig. 18a), in agreement with results simulated by CCSM (Fig. 17a). However, the anomalous upward-propagating Rossby waves are confined in the midlatitude troposphere during the MH and LGM winter (Figs. 18b,c). Overall, the simulation results of two models show that the increase in fall snow depth leads to anomalous upward propagation of Rossby waves persistently during the PI, MH, and LGM winter.

It is revealed that the increased fall snow depth in the same period generates anomalous upward-propagating Rossby waves persisting until winter. The ice sheets increased largely during the LGM because of a cooler climate. Correspondingly, the snow depth increased gradually in a long cold period. The snow depth may denote ice sheet thickness over land to some extent, especially in a cold climate state. Thus, the role of the increased fall snow depth during the LGM compared to the PI is further explored. Figure 19 shows the regression coefficients of LGM winter zonal-mean WAF on the increment of autumn snow depth indices between the LGM and PI. The areas reaching the 90% confidence level are shaded. It is evident that the increment of

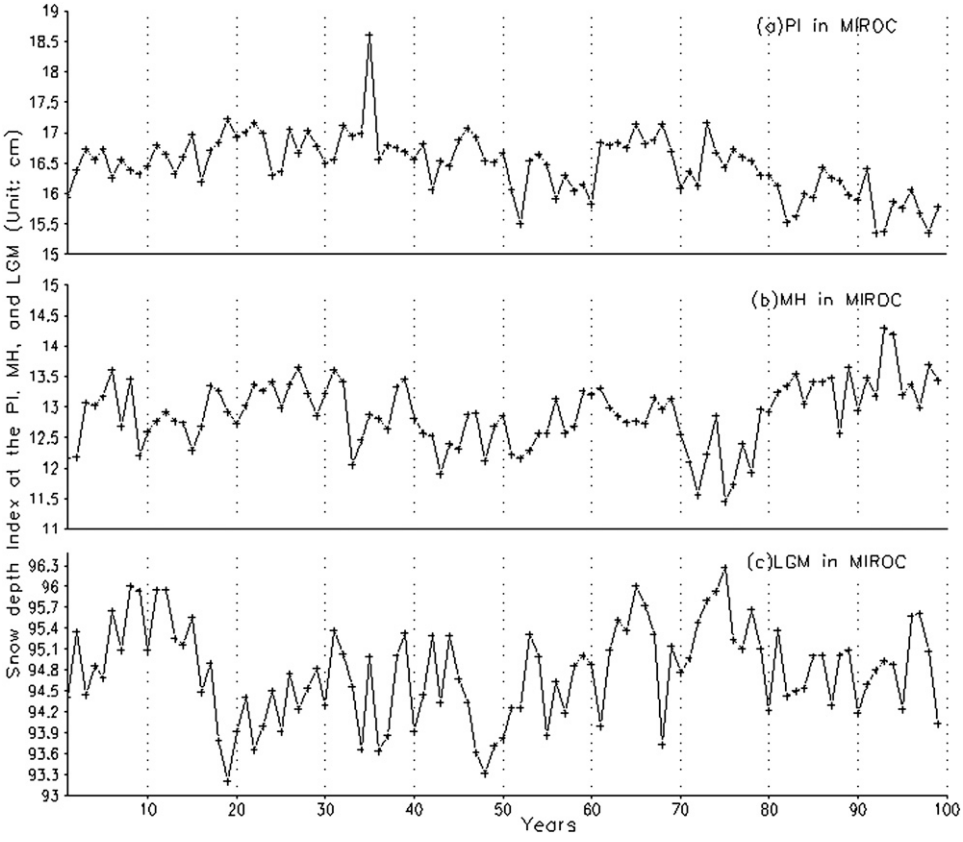

FIG. 16. As in Fig. 15, but for MIROC.

autumn snow depth generates statistically significant anomalous upward propagation of Rossby waves during the LGM winter, which prevails from the mid- and high-latitude troposphere through the stratosphere in CCSM (Fig. 19a). However, in MIROC it extends from the midlatitude troposphere to the stratosphere (Fig. 19b). This suggests that the large increase in fall snow enhances anomalous upward-propagating Rossby waves during the LGM compared to the PI. It is consistent with previously mentioned result that the upward propagation of Rossby waves during the LGM is much stronger than that during the PI.

5. Summary and conclusions

In this study, we compared changes in the AO during the MH and LGM from the PI using four atmosphere–ocean coupled model simulations. This comparison confirms previous conclusions, and also reveals some novel findings.

For the control simulation (PI), the AO pattern simulated by all models shows features very similar to those of present-day observed results (TW98). The CCSM model accurately reproduces vertical AO structures similar to those observed in TW00 and performs better than MIROC. During the MH, important external forcings are derived from seasonal changes in the incoming solar radiation (insolation) caused by known changes in orbital parameters. The NH mean winter SAT is slightly lower during the MH than during the PI because of lower insolation. Meanwhile, the intensity of the AO slightly decreases in comparison with the PI. AO signals in the latitude–pressure cross section of zonal-mean zonal wind, geopotential height, and temperature exhibit small changes, including the weakening of the polar westerlies and the polar vortex, the downward displacement of the polar westerly center, and the warming of the cold polar cap region from the lower troposphere to the stratosphere.

During the LGM, the climate in the NH experiences a severe cooling. The simulated AO patterns in all models show different features from those in the PI simulation. The centers of negative anomalies near the pole and positive anomalies at middle latitudes weaken noticeably, and the positive anomalies at middle latitudes

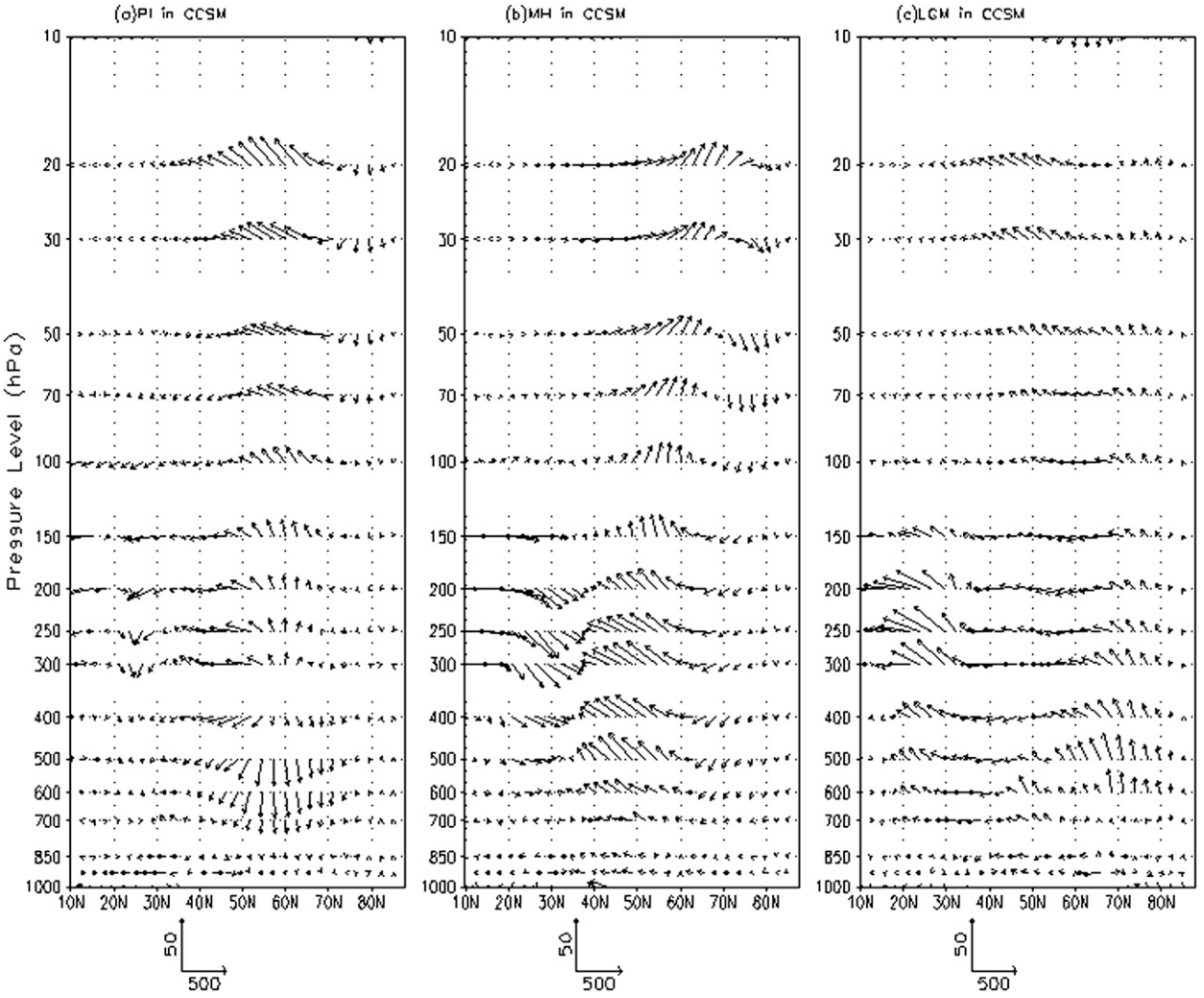

FIG. 17. Latitude–pressure cross section of the regression coefficients of winter zonal-mean WAF (arrow) on autumn snow depth indices from CCSM simulation for the (a) PI, (b) MH, and (c) LGM. The horizontal (vertical) scale of arrows is shown at the bottom and represents 500 (50) $m^2 s^{-2}$.

are shifted equatorward. All models consistently show that the intensity of the AO decreases considerably during the LGM. The vertical structure of the AO during the LGM is characterized by a distinct weakening of the polar vortex and polar westerlies. Note also that the westerly center is displaced downward and southward into the midlatitudes upper troposphere and confined in the upper troposphere. The polar cap region still remains cold in the troposphere, whereas it becomes anomalously warm in the stratosphere.

In general, an increase in planetary wave activity leads to an increase in dynamic adiabatic heating and a warming of polar stratosphere, indicative of a decrease in meridional temperature gradient. The polar vortex thus becomes weaker. We showed in this paper that the enhanced upward-propagating stationary Rossby waves are responsible for the weakening of the AO during the MH and LGM. The upward propagation of Rossby waves during the MH is stronger than that simulated for the PI. This results in small weakening of the AO during the MH. During the LGM, the upward propagation of Rossby waves is much stronger than that during the PI. This causes the warming of the polar stratosphere, a decrease of meridional temperature gradient, and finally considerable weakening of the AO. Additionally, we suggest that the anomalous snow cover in the NH plays an important role in the vertical propagation of stationary Rossby waves. During the LGM, a large increase in fall snow depth generates anomalous upward propagation of Rossby waves; these waves persist until winter

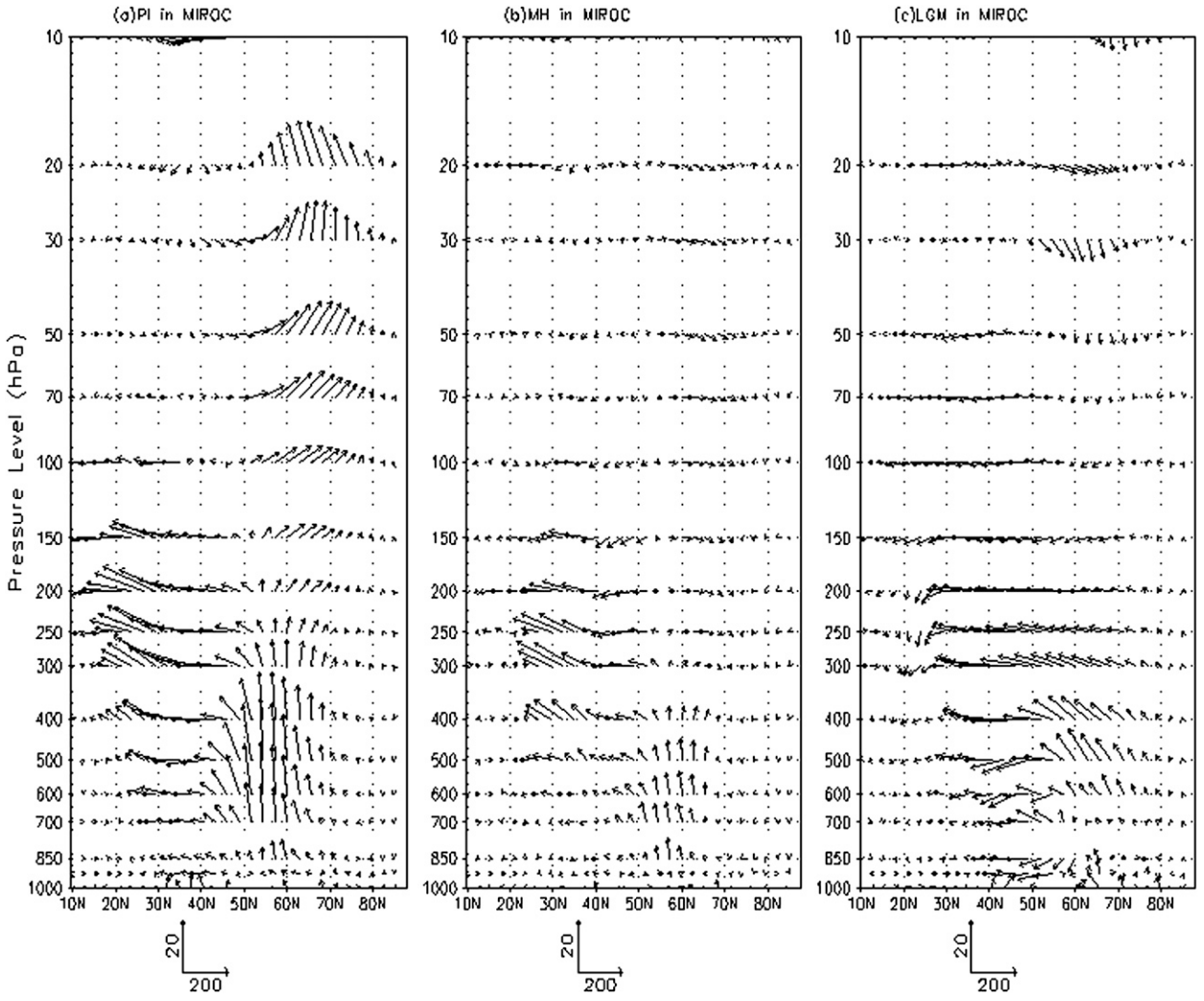

FIG. 18. As in Fig. 17, but for MIROC. The horizontal (vertical) scale of arrows is shown at the bottom and represents 200 (20) $m^2 s^{-2}$.

and intensify the upward-propagating stationary Rossby waves relative to the PI.

The AO appears to be sensitive to the background climate state. When the climate becomes slightly cold during the MH, a small decrease in AO amplitude occurs. Furthermore, the intensity of the AO is substantially weakened during the LGM when the climate becomes intensely cold. For the opposite climate scenario (i.e., global warming), the intensity of the AO has increased and has consequently accelerated warming for the last 30 yr as shown by Thompson et al. (2000) and Thompson and Wallace (2001). Studies to date have focused on the trend of the AO when anthropogenic influence leads to more serious global warming in the future (Paeth and Hense 1999; Shindell et al. 1999; Fyfe et al. 1999; Cohen and Barlow 2005). Additional work and additional scenario simulations should be performed to confirm the intensification of the AO and to fully assess how intensification of the AO could affect extreme climate events in the future.

Acknowledgments. We thank three anonymous reviewers for their comments that helped to improve the quality of the paper. We would like to appreciate PMIP2 members for providing data. This study was supported by the Project of Integrated Research on the Composition of Polar Atmosphere and Climate Change (COMPAC; Grant PE10030), the Paleoclimate Modelling Study for Polar Regions (Grant PE09120) of the Korea Polar Research Institute, and the National Natural Science Foundation of China (Grants 40705026 and 40675049).

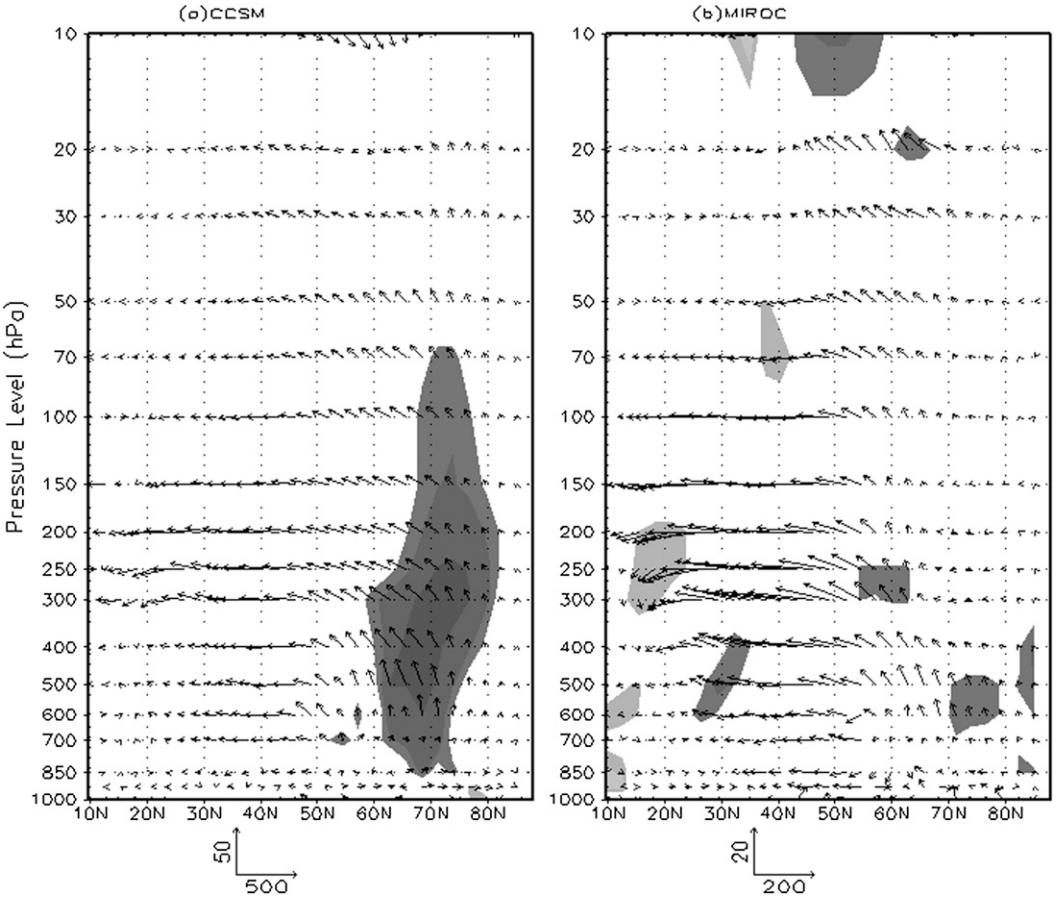

FIG. 19. The regression coefficients of LGM winter zonal-mean WAF (arrow) on the increment of autumn snow depth indices between the LGM and PI for (a) CCSM and (b) MIROC. Shaded areas indicate 90%, 95%, and 99% confidence levels. The horizontal (vertical) scale of arrows is shown at the bottom and represents 500 (50) or 200 (20) $m^2 s^{-2}$.

REFERENCES

Andrews, D. G., J. R. Holton, and C. B. Leovy, 1987: *Middle Atmosphere Dynamics*. Academic Press, 489 pp.

Berger, A. L., 1978: Long-term variations of caloric insolation resulting from the earth's orbital elements. *Quat. Res.,* **9,** 139–167.

Braconnot, P., and Coauthors, 2007a: Results of PMIP2 coupled simulations of the mid-Holocene and Last Glacial Maximum—Part 1: Experiments and large-scale features. *Climate Past,* **3,** 261–277.

——, and Coauthors, 2007b: Results of PMIP2 coupled simulations of the mid-Holocene and Last Glacial Maximum—Part 2: Feedbacks with emphasis on the location of the ITCZ and mid- and high latitudes heat budget. *Climate Past,* **3,** 279–296.

Brewer, S., J. Guiot, and F. Torre, 2007: Mid-Holocene climate change in Europe: A data-model comparison. *Climate Past,* **3,** 499–512.

Chen, W., and R. H. Huang, 2005: The three-dimensional propagation of quasi-stationary planetary waves in the Northern Hemisphere winter and its interannual variations (in Chinese). *Chin. J. Atmos. Sci.,* **29,** 137–146.

Cohen, J., and M. Barlow, 2005: The NAO, the AO, and global warming: How closely related? *J. Climate,* **18,** 4498–4512.

——, ——, P. Kushner, and K. Saito, 2007: Stratosphere–troposphere coupling and links with Eurasian land surface variability. *J. Climate,* **20,** 5335–5343.

Crucifix, M., P. Braconnot, S. P. Harrison, and B. Otto-Bliesner, 2005: Second phase of Paleoclimate Modelling Intercomparison Project. *Eos, Trans. Amer. Geophys. Union,* **86,** 264.

Davis, B. A. S., S. Brewer, A. C. Stevenson, and J. Guiot, 2003: The temperature of Europe during the Holocene reconstructed from pollen data. *Quat. Sci. Rev.,* **22,** 1701–1716.

DeWeaver, E., and S. Nigam, 2000: Zonal-eddy dynamics of the North Atlantic Oscillation. *J. Climate,* **13,** 3893–3914.

Fyfe, J. C., G. J. Boer, and G. M. Flato, 1999: The Arctic and Antarctic oscillations and their projected changes under global warming. *Geophys. Res. Lett.,* **26,** 1601–1604.

Gladstone, R. M., and Coauthors, 2005: Mid-Holocene NAO: A PMIP2 model intercomparison. *Geophys. Res. Lett.,* **32,** L16707, doi:10.1029/2005GL023596.

Gong, D. Y., S. W. Wang, and J. H. Zhu, 2001: East Asian winter monsoon and Arctic Oscillation. *Geophys. Res. Lett.,* **28,** 2073–2076.

Gordon, C., C. Cooper, C. A. Senior, H. Banks, J. M. Gregory, T. C. Johns, J. F. B. Mitchell, and R. A. Wood, 2000: The simulation of SST, sea-ice extents and ocean heat transports in a version of the Hadley Centre model without flux adjustments. *Climate Dyn.,* **16,** 147–168.

Harrison, S. P., P. Bracannot, S. Joussaume, C. D. Hewitt, and R. J. Stouffer, 2002: Fourth international workshop of the Palaeoclimate Modelling Intercomparison Project (PMIP): Launching PMIP Phase II. *Eos, Trans. Amer. Geophys. Union,* **83,** 447.

Hasumi, H., and S. Emori, Eds., 2004: K-1 coupled GCM (MIROC) description. University of Tokyo Center for Climate System Research K-1 Tech. Rep. 1, 39 pp.

Hu, Y. Y., and K. K. Tung, 2003: Possible ozone-induced long-term changes in planetary wave activity in late winter. *J. Climate,* **16,** 3027–3038.

Kageyama, M., and Coauthors, 2006: Last Glacial Maximum temperatures over the North Atlantic, Europe and western Siberia: A comparison between PMIP models, MARGO sea–surface temperatures and pollen-based reconstructions. *Quat. Sci. Rev.,* **25,** 2082–2102, doi:10.1016/j.quascirev.2006.02.010.

Kalnay, E., and Coauthors, 1996: The NCEP/NCAR 40-Year Reanalysis Project. *Bull. Amer. Meteor. Soc.,* **77,** 437–471.

Kerr, R. A., 1999: A new force in high-latitude climate. *Science,* **284,** 241–242.

Kim, S.-J., T. J. Crowley, D. J. Erickson, B. Govindasamy, P. B. Duffy, and B. Y. Lee, 2008: High-resolution climate simulation of the Last Glacial Maximum. *Climate Dyn.,* **31,** 1–16, doi:10.1007/s00382-007-0332-z.

Lü, J.-M., J.-H. Ju, S.-J. Kim, J.-Z. Ren, and Y.-X. Zhu, 2008: Arctic Oscillation and the autumn/winter snow depth over the Tibetan Plateau. *J. Geophys. Res.,* **113,** D14117, doi:10.1029/2007JD009567.

Marti, O., and Coauthors, 2005: The new IPSL climate system model: IPSL-CM4. Institut Pierre Simon Laplace Note du Pôle de Modélisation 26, 86 pp.

Newman, P. A., J. F. Gleason, R. D. McPeters, and R. S. Stolarski, 1997: Anomalously low ozone over the Arctic. *Geophys. Res. Lett.,* **24,** 2689–2692.

Otto-Bliesner, B. L., E. C. Brady, G. Clauzet, R. Tomas, S. Levis, and Z. Kothavala, 2006: Last Glacial Maximum and Holocene climate in CCSM3. *J. Climate,* **19,** 2526–2544.

Paeth, H., and A. Hense, 1999: Climate change signals in the North Atlantic Oscillation. *CLIVAR Exchanges,* No. 4, International CLIVAR Project Office, Southampton, United Kingdom, 25–29.

Plumb, R. A., 1985: On the three-dimensional propagation of stationary waves. *J. Atmos. Sci.,* **42,** 217–229.

PMIP, 2000: *Paleoclimate Modeling Intercomparison Project (PMIP): Proceedings of the Third PMIP Workshop*. WCRP-111, WMO/TD-1007, World Meteorological Organisation and World Climate Research Programme 271 pp.

Rimbu, N., G. Lohmann, J.-H. Kim, H. W. Arz, and R. Schneider, 2003: Arctic/North Atlantic Oscillation signature in Holocene sea surface temperature trends as obtained from alkenone data. *Geophys. Res. Lett.,* **30,** 1280, doi:10.1029/2002GL016570.

Ringler, T. D., and K. H. Cook, 1999: Understanding the seasonality of orographically forced stationary waves: Interaction between mechanical and thermal forcing. *J. Atmos. Sci.,* **56,** 1154–1174.

Saito, K., J. Cohen, and D. Entekhabi, 2001: Evolution of atmospheric response to early-season Eurasian snow cover anomalies. *Mon. Wea. Rev.,* **129,** 2746–2760.

Shindell, D. T., R. L. Miller, G. A. Schmidt, and L. Pandolfo, 1999: Simulation of recent northern winter climate trends by greenhouse-gas forcing. *Nature,* **399,** 452–455.

Thompson, D. W. J., and J. M. Wallace, 1998: The Arctic Oscillation signature in the wintertime geopotential height and temperature fields. *Geophys. Res. Lett.,* **25,** 1297–1300.

——, and ——, 2000: Annular modes in the extratropical circulation. Part I: Month-to-month variability. *J. Climate,* **13,** 1000–1016.

——, and ——, 2001: Regional climate impacts of the Northern Hemisphere annular mode and associated climate trends. *Science,* **293,** 85–89.

——, ——, and G. C. Hegerl, 2000: Annular modes in the extratropical circulation. Part II: Trends. *J. Climate,* **13,** 1018–1036.

Waugh, D. W., W. J. Randel, S. Pawson, P. A. Newman, and E. R. Nash, 1999: Persistence of the lower stratospheric polar vortices. *J. Geophys. Res.,* **104,** 27 191–27 202.

Weber, S. L., and Coauthors, 2007: The modern and glacial overturning circulation in the Atlantic Ocean in PMIP coupled model simulations. *Climate Past,* **3,** 51–64.

Wu, B., and J. Wang, 2002: Possible impacts of winter Arctic Oscillation on Siberian high, the East Asian winter monsoon and sea-ice extent. *Adv. Atmos. Sci.,* **19,** 297–320.

Zheng, W., P. Braconnot, E. Guilyardi, U. Merkel, and Y. Yu, 2008: ENSO at 6ka and 21ka from ocean–atmosphere coupled model simulations. *Climate Dyn.,* **30,** 745–762, doi:10.1007/s00382-007-0320-3.